Article

SOURCE DATA | TRANSPARENT PROCESS

THE EMBO JOURNAL

ARF2-PIF5 interaction controls transcriptional reprogramming in the ABS3-mediated plant senescence pathway

Hui Xue[1,†], Jingjing Meng[1,†], Pei Lei[1], Yongxin Cao[1], Xue An[1], Min Jia[1,‡], Yan Li[1], Haofeng Liu[1], Jen Sheen[3,4], Xiayan Liu[1,3,4] & Fei Yu[1,2,*]

Abstract

One of the hallmarks of plant senescence is the global transcriptional reprogramming coordinated by a plethora of transcription factors (TFs). However, mechanisms underlying the interactions between different TFs in modulating senescence remain obscure. Previously, we discovered that plant *ABS3* subfamily MATE transporter genes regulate senescence and senescence-associated transcriptional changes. In a genetic screen for mutants suppressing the accelerated senescence phenotype of the gain-of-function mutant *abs3-1D*, AUXIN RESPONSE FACTOR 2 (ARF2) and PHYTOCHROME-INTERACTING FACTOR 5 (PIF5) were identified as key TFs responsible for transcriptional regulation in the ABS3-mediated senescence pathway. ARF2 and PIF5 (as well as PIF4) interact directly and function interdependently to promote senescence, and they share common target genes such as key senescence promoting genes *ORESARA 1* (*ORE1*) and *STAY-GREEN 1* (*SGR1*) in the ABS3-mediated senescence pathway. In addition, we discovered reciprocal regulation between ABS3-subfamily MATEs and the ARF2 and PIF5/4 TFs. Taken together, our findings reveal a regulatory paradigm in which the ARF2-PIF5/4 functional module facilitates the transcriptional reprogramming in the ABS3-mediated senescence pathway.

Keywords ABS3; ARF2; PIF5; senescence; transcriptional regulation
Subject Category Plant Biology
DOI 10.15252/embj.2022110988 | Received 21 February 2022 | Revised 17 July 2022 | Accepted 21 July 2022 | Published online 9 August 2022
The EMBO Journal (2022) 41: e110988

Introduction

Senescence, or aging, is an integral, active, and final chapter of life. For sessile land plants, a coordinated senescence program is essential for nutrient repurposing, reproduction, and the survival of the species (Schippers *et al*, 2015; Woo *et al*, 2019). The integration of developmental, hormonal, and environmental regulatory pathways ensure plant senescence is executed in an orderly fashion (Schippers *et al*, 2015). Environmental factors, both abiotic and biotic, also drastically impact senescence. The deprivation of light under shading or dark conditions induces precocious senescence (Liebsch & Keech, 2016; Kamranfar *et al*, 2018). Premature senescence due to abiotic and biotic stresses can negatively impact both plant growth and crop production (Guo & Gan, 2014).

One central hallmark of plant senescence is the transcriptome-wide reprogramming of gene expressions, including the induction of many senescence-associated genes (*SAGs*; Breeze *et al*, 2011; Buchanan-Wollaston *et al*, 2005; Guo *et al*, 2004; Guo & Gan, 2012; Guo & Gan, 2014; Kim *et al*, 2016; Liebsch & Keech, 2016; Lin & Wu, 2004; Woo *et al*, 2019; Woo *et al*, 2016). It is evident that a complex array of transcription factors (TFs) are involved in the transcriptional regulation of senescence. On one hand, many TF genes are *SAGs* and their expression is activated as part of the transcriptome reconfiguration during senescence (Lin & Wu, 2004; Kim *et al*, 2016). On the other hand, molecular genetics investigations have established an increasing number of TFs as genetic regulators of senescence (Woo *et al*, 2019). In light signaling, red light suppresses senescence by converting the Pr form of phytochrome B (phyB) to the active Pfr form, which subsequently inhibits the bHLH family TFs PHYTOCHROME-INTERACTING FACTOR 4 (PIF4) and PIF5, both positive regulators of senescence (Sakuraba *et al*, 2014; Song *et al*, 2014; Zhang *et al*, 2015). In the ethylene pathway, plant-specific TF ETHYLENE INSENSITIVE 3 (EIN3) acts downstream of EIN2 to promote senescence (Sakuraba *et al*, 2014). In the ABA pathway, the bZIP TFs ABA INSENSITIVE 5 (ABI5) and ENHANCED EM LEVEL (EEL) as well as the NAC family TF NAC-LIKE, ACTIVATED BY AP3/PI (NAP), work together to promote senescence (Sakuraba *et al*, 2014; Yang *et al*, 2014). In addition, AUXIN RESPONSE FACTOR 2 (ARF2), an ARF family of TFs

1 State Key Laboratory of Crop Stress Biology for Arid Areas and College of Life Sciences, Northwest A&F University, Yangling, China
2 Institute of Future Agriculture, Northwest A&F University, Yangling, China
3 Department of Molecular Biology and Centre for Computational and Integrative Biology, Massachusetts General Hospital, Boston, MA, USA
4 Department of Genetics, Harvard Medical School, Boston, MA, USA
*Corresponding author. Tel: +86 29 87091935; E-mail: feiyu@nwafu.edu.cn
†These authors contributed equally to this work
‡Present address: Department of Plant and Microbial Biology, University of California, Berkeley, Berkeley, CA, USA

presumably involved in auxin signaling, was identified as a regulator of senescence based on the delayed senescence phenotype of the loss-of-function *arf2* mutants (Ellis *et al*, 2005; Okushima *et al*, 2005; Lim *et al*, 2010). Through the *oresara* (*ore*; Korean meaning long-living) mutant screen, the NAC family TF ORE1 was identified as a key TF promoting senescence (Kim *et al*, 2009, 2018; Durian *et al*, 2020). Current data suggest that independent or sequential actions of upstream TFs, PIF4/PIF5, ABI5, and EIN3 converge on ORE1 to facilitate senescence (Sakuraba *et al*, 2014). It is evident that extensive cross-talks occur between these TF cascades to ensure the highly organized transcriptome reprogramming during senescence (Woo *et al*, 2019).

To dissect the molecular mechanisms that modulate the signaling networks in plant senescence, we have established a highly reproducible system in which senescence is induced in *Arabidopsis* seedlings with the carbon (C)-deprivation treatment (Jia *et al*, 2019). We have shown that the ABS3 subfamily of MATE transporters acts as positive regulators of plant senescence. A gain-of-function mutant allele of *ABS3*, *abs3-1D*, in which the expression of *ABS3* is activated by an activation tagging T-DNA upstream of the *ABS3* gene, displays an accelerated senescence phenotype while the knockout of four *ABS3* subfamily genes in *mateq* quadruple mutant drastically inhibited senescence (Wang *et al*, 2015a; Jia *et al*, 2019). The ABS3 subfamily transporters reside in late endosome, interact in a non-canonical way with AUTOPHAGY 8 (ATG8), and facilitate degradation through the vacuole (Jia *et al*, 2019; Zentgraf, 2019). Interestingly, the expressions of several *SAGs* were precociously induced in *abs3-1D*, but delayed in *mateq*, upon C-deprivation. The natural question is that how does a cytoplasmic degradation process mediated by ABS3 triggers gene expression responses in the nucleus, and we hypothesized that a retrograde signaling pathway operates from the cytoplasm to the nucleus to regulate nuclear gene expression in the ABS3-mediated senescence pathway.

In this work, taking a molecular genetics approach, we identified extragenic suppressor mutations in *ARF2* and *PIF5* that reversed the precocious senescence phenotype of *abs3-1D*, as well as the ectopic *SAG* activation in *abs3-1D* at the molecular level. In addition, ARF2 physically interacts with PIF5 and PIF4, and together they control the transcriptional response in the ABS3-mediated senescence pathway. We revealed previously unrecognized molecular mechanisms of functional interdependency between ARF2 and PIF5 in promoting senescence. Furthermore, we uncovered reciprocal regulations between ABS3 subfamily MATEs and the ARF2 and PIF5/4 TFs. Together, our findings reveal a senescence regulatory paradigm in which the ARF2-PIF5/4 TF functional module facilitates the transcriptional regulation in the endosomal ABS3-mediated senescence pathway.

Results

ARF2 and *PIF5* are required for the ABS3-mediated senescence pathway

To identify signaling components in the ABS3-mediated senescence pathway, we carried out ethyl methanesulfonate (EMS) mutagenesis in the *abs3-1D* background and screened for suppressor mutants that could reverse the accelerated senescence phenotype of *abs3-1D* under C-deprivation. Two non-allelic and recessive suppressor lines, designated *FD11-55* and *FD18-70*, were identified (Fig 1A and B). The activated expressions of *ABS3* were validated in *FD11-55* and *FD18-70*, respectively, ruling out the possibility of suppression through transcriptional silencing (Fig 1C and D). Phenotypically, the suppressor mutations in *FD11-55* and *FD18-70* significantly reversed the accelerated senescence of *abs3-1D*, indicated by the relative contents of chlorophyll and total cellular proteins under C-deprivation (Fig 1E and F). Moreover, the ectopically induced expressions of *SAGs*, such as *ORESARA 1* (*ORE1*) and *STAY-GREEN 1* (*SGR1*; Armstead *et al*, 2007; Kim *et al*, 2009), in *abs3-1D* under C-deprivation were also greatly reduced in *FD11-55* and *FD18-70*, respectively (Fig 1G and H). To identify the molecular lesions in *FD11-55* and *FD18-70*, suppressor lines were backcrossed with the wild type (WT) and whole-genome resequencing of pooled genomic DNAs of suppressor mutants from the F2 segregating population was carried out. In *FD11-55*, a C to T nonsense mutation was identified in the *AUXIN RESPONSE FACTOR 2* (*ARF2*/At5g62000) gene, converting the codon CAA for Q101 to a stop codon (Fig 1I). In *FD18-70*, a C to T nonsense mutation converting the codon CAG for Q159 to a stop codon in the *PHYTOCHROME-INTERACTING FACTOR 5* (*PIF5*/At3g59060) gene was identified (Fig 1J).

To verify that the mutations we identified in *ARF2* and *PIF5* are the causal mutations in *FD11-55* and *FD18-70*, respectively, we expressed *ARF2-GFP* in *FD11-55* and *PIF5-GFP* in *FD18-70* under the control of their endogenous promoters (*pARF2:ARF2-GFP* and *pPIF5:PIF5-GFP*), respectively. For both complementation assays, we obtained multiple transgenic lines that restored the accelerated senescence phenotype of *abs3-1D* (Fig EV1A–F). The delayed senescence phenotypes in single mutants of *arf2-20* or *pif5-10* under C-deprivation were also reversed by the introduction of *pARF2:ARF2-GFP* and *pPIF5:PIF5-GFP* (Fig EV1G–L). Finally, soil-grown single mutants of *arf2-20* and *pif5-10* also showed delayed natural senescence compared with the WT, as reported, and suppressed the precocious natural senescence in *abs3-1D* (Appendix Fig S1A and B; Ellis *et al*, 2005; Lim *et al*, 2010; Okushima *et al*, 2005; Sakuraba *et al*, 2014; Song *et al*, 2014; Zhang *et al*, 2015). Together, these data establish that ARF2 and PIF5 are required for the ABS3-mediated senescence during both C-deprivation-induced and natural senescence.

ARF2 and PIF5 control the transcriptional reprogramming in the ABS3-mediated senescence pathway

Given that ARF2 and PIF5 are both TFs, we investigated whether they are responsible for the aberrant transcriptional activation of *SAGs* in the ABS3-mediated senescence pathway (Jia *et al*, 2019). To this end, transcriptome profiles of WT, *abs3-1D*, *arf2-20 abs3-1D*, *arf2-20*, *pif5-10 abs3-1D*, and *pif5-10* seedlings before and after 4-day C-deprivation were analyzed with RNA-seq. First, we identified 2,587 differentially expressed genes (DEGs; $|\log_2 FC| > 0.6$, padj<0.01) between *abs3-1D* and WT under C-deprivation. Interestingly, the majority of these DEGs (2,412 of 2,587) were only affected by the *abs3-1D* mutation under C-deprivation, but not differentially expressed in samples before C-deprivation, suggesting a highly specific transcriptional response in *abs3-1D* upon C-deprivation (Dataset EV1). The most enriched Gene Ontology (GO) terms in *abs3-1D* up-regulated genes included leaf senescence

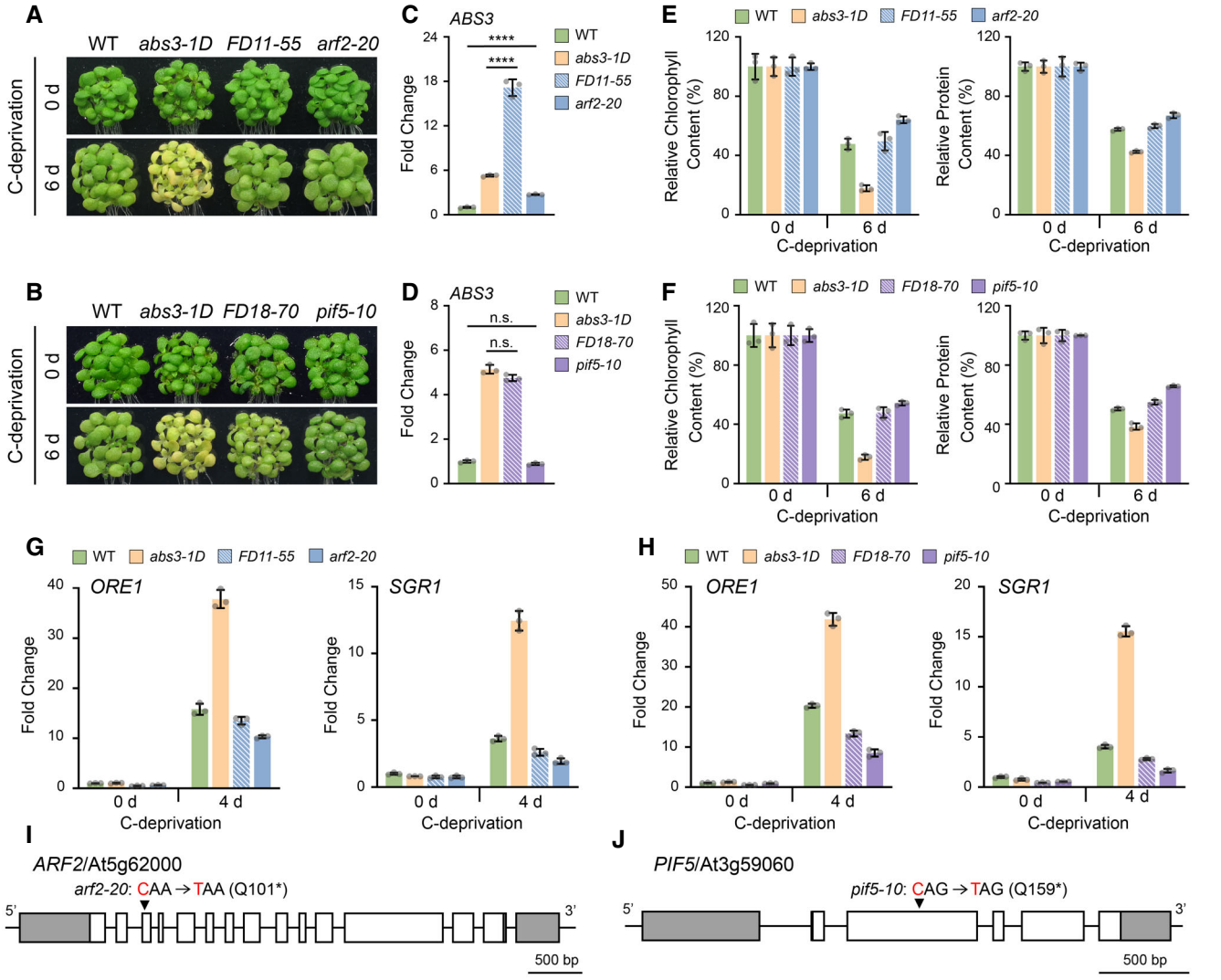

Figure 1. *ARF2* and *PIF5* are required for ABS3-mediated senescence.

A Seedlings of WT, *abs3-1D*, *FD11-55*, and *arf2-20* before and after 6 days C-deprivation.

B Seedlings of WT, *abs3-1D*, *FD18-70*, and *pif5-10* before and after 6 days C-deprivation.

C, D RT-qPCR analysis of *ABS3* expression levels in 7-day-old seedlings of the same genotypes as shown in A (C) and B (D). Fold changes were calculated with respect to the expression level in the WT. two-tailed *t* test, ****$P < 0.0001$, n.s., not significant.

E, F Chlorophyll and total cellular protein content reduction in genotypes shown in A (E) and B (F) after 6 days C-deprivation.

G, H RT-qPCR analysis of *ORE1* and *SGR1* expression levels in genotypes shown in A (G) and B (H) before and after 4 days C-deprivation. Fold changes were calculated with respect to the expression level in the WT before C-deprivation.

I, J Suppressor mutation sites in *FD11-55* (I) and *FD18-70* (J). In the gene model, boxes and lines represent exons and introns, respectively. 5′- and 3′-untranslated regions (UTRs) are shaded in gray. The arrow head indicates the position of the suppressor mutation site. In (C–H), data are means ± standard deviation (s.d.) of three biological replicates.

(Fig 2A). In addition, genes involved in senescence-promoting processes and plant hormones, such as defense response, abscisic acid, jasmonic acid, and salicylic acid, were also enriched in *abs3-1D* up-regulated genes (Fig 2A). Conversely, the most enriched GO terms in *abs3-1D* down-regulated genes were processes related to photosynthesis, consistent with the accelerated chlorophyll degradation and senescence phenotype of *abs3-1D* during C-deprivation (Fig 2B). These findings indicate that the ABS3-mediated senescence pathway entails transcriptome reprogramming and transcriptional regulation.

Next, we analyzed the expression profiles of *abs3-1D*-regulated genes in *arf2-20* and *pif5-10* backgrounds, respectively. Under C-deprivation, the impact of *abs3-1D* on gene expression was almost completely abolished in the *arf2-20* background (*arf2-20 abs3-1D* vs. *arf2-20*) when compared with the WT background (*abs3-1D* vs. WT; Fig 2C). The differential expressions of 97.7% of the *abs3-1D* up-regulated genes (1,309 of 1,340) and 97.8% of the *abs3-1D* down-regulated genes (1,219 of 1,247) in the WT background were abolished or reversed in the *arf2-20* background (Fig 2D; Dataset EV2). The *pif5-10* background showed a similar albeit weaker effect on

the *abs3-1D*-regulated genes compared with the *arf2-20* background under C-deprivation (Fig 2C). Differential expressions of 72.5% of the *abs3-1D* up-regulated genes (971 of 1,340) and 86.2% of the *abs3-1D* down-regulated genes (1,075 of 1,247) in the WT background were diminished or reversed in the *pif5-10* background (Fig 2D; Dataset EV3). These results demonstrate that ARF2 and PIF5 play essential roles in mediating the transcriptome reprogramming in *abs3-1D* under C-deprivation.

To reveal the molecular signatures of ARF2- and PIF5-regulated genes in the ABS3-mediated senescence pathway, we identified 3,448 ARF2-regulated genes (*abs3-1D* vs. *arf2-20 abs3-1D*) and 2,745 PIF5-regulated genes (*abs3-1D* vs. *pif5-10 abs3-1D*) in the

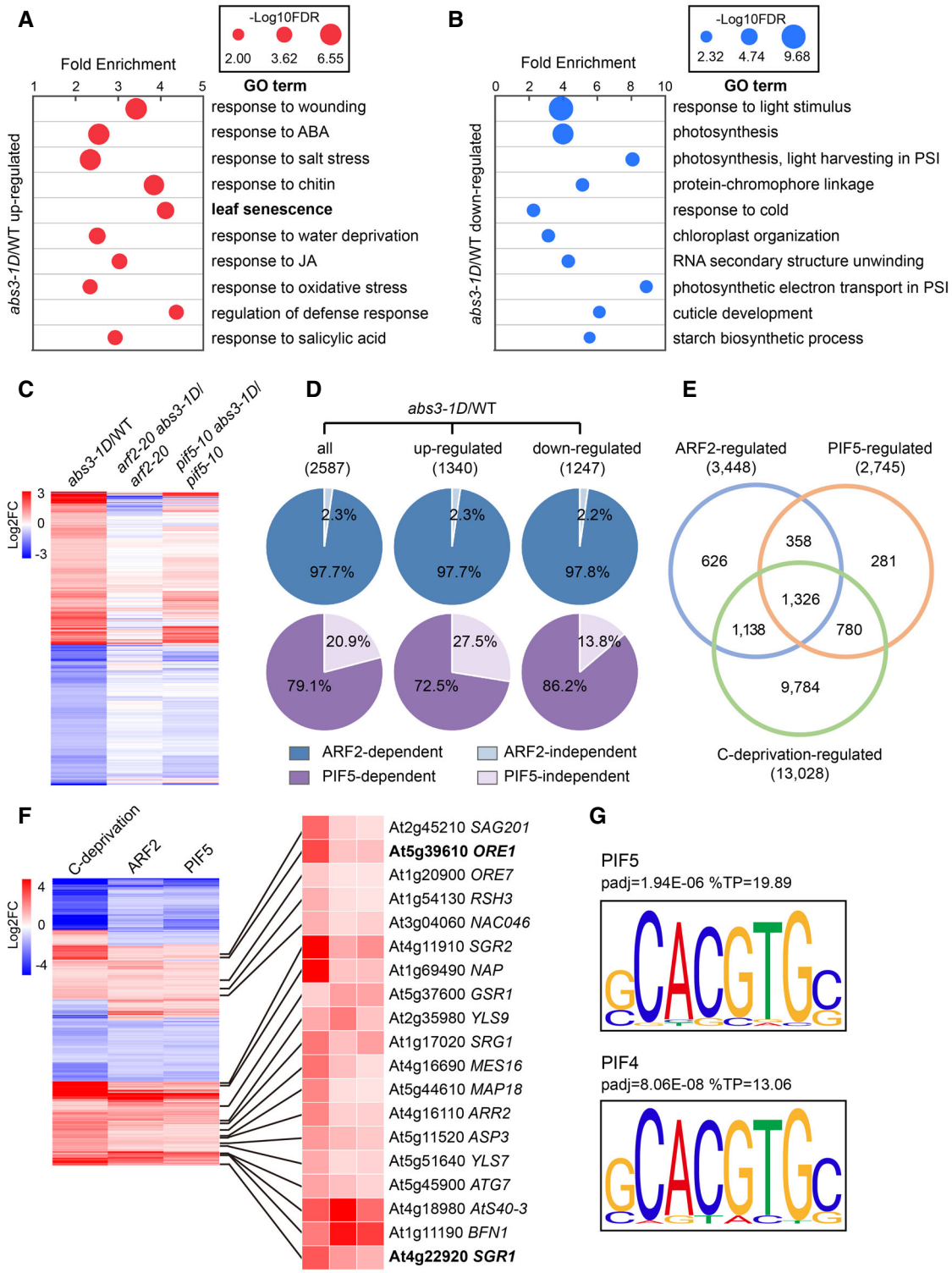

Figure 2.

Figure 2. ARF2 and PIF5 control the transcriptional reprogramming in the ABS3-mediated senescence pathway.

A, B Top 10 significantly enriched GO terms derived from genes that are up-regulated (A) or down-regulated (B) in *abs3-1D* seedlings compared with the WT under C-deprivation. Enriched GO terms were ranked based on their false discovery rate (FDR).

C Heatmap of log2FC values of 2,587 ABS3-regulated genes (*abs3-1D* vs. WT) under C-deprivation in indicated comparisons.

D Percentage of ARF2- or PIF5-dependent ABS3-regulated genes under C-deprivation. Genes that were not significantly up- or down-regulated by *abs3-1D* in the *arf2-20* (*arf2-20 abs3-1D* vs. *arf2-20*) or *pif5-10* (*pif5-10 abs3-1D* vs. *pif5-10*) background under C-deprivation were defined as ARF2- or PIF5-dependent ABS3-regulated genes, respectively.

E Significant overlap between ARF2-, PIF5-, and C-deprivation-regulated genes in the *abs3-1D* background.

F Heatmap of log2FC values of 1,326 ARF2, PIF5, and C-deprivation co-regulated genes in indicated comparisons. C-deprivation: *abs3-1D* 4 days C-deprivation vs. *abs3-1D* 0 day C-deprivation; ARF2: *abs3-1D* vs. *arf2-20 abs3-1D* after 4 days C-deprivation; PIF5: *abs3-1D* vs. *pif5-10 abs3-1D* after 4 days C-deprivation. Enlarged were expression changes of senescence genes identified in DAVID GO analysis (https://david.ncifcrf.gov/).

G PIF5 and PIF4 binding motifs were over-represented in the promoter regions of ARF2, PIF5, and C-deprivation co-regulated genes. Enriched motifs were identified with the AME tool in MEME Suite 5.3.3 (https://meme-suite.org/meme/tools/ame) using 1,000 bp promoter sequences.

abs3-1D background. A significant overlap (1,684 genes) was observed between ARF2-regulated and PIF5-regulated genes (Fig 2E; Dataset EV4). Moreover, the majority of the genes co-regulated by ARF2 and PIF5 (1,326 of 1,684) were also regulated in similar manners by C-deprivation in the *abs3-1D* background (*abs3-1D* 4 days C-deprivation vs. *abs3-1D* 0 day C-deprivation; Fig 2E and F). This subset of 1,326 genes co-regulated by C-deprivation, ARF2, and PIF5 in the *abs3-1D* background includes many known *SAGs*, such as *ORE1* and *SGR1* (Fig 2F). Finally, we identified conserved over-represented *cis*-elements in the promoters of genes co-regulated by C-deprivation, ARF2, and PIF5 in the *abs3-1D* background. G-box, a conserved binding motif for PIF5 and PIF4, was significantly enriched (Fig 2G; Hornitschek *et al*, 2012). These findings suggest that a common set of genes are regulated by ARF2, PIF5, and C-deprivation in the *abs3-1D* background.

PIF5 and PIF4 share redundant roles in the ABS3-mediated senescence pathway and interact directly with ARF2

Given the conserved nature of PIF5 and PIF4, we next tested genetically whether PIF4 is also involved in the ABS3-mediated senescence pathway (Leivar & Monte, 2014; Pfeiffer *et al*, 2014; Paik *et al*, 2017; Pham *et al*, 2018). A T-DNA insertion allele of *PIF4*, *pif4-2* (SAIL_1288_E07), was crossed with *pif5-10*, *abs3-1D*, and *pif5-10 abs3-1D* to obtain higher order mutants (Leivar *et al*, 2008a). *pif4-2* alone also showed resistant to C-deprivation-induced senescence, albeit weaker than that of *pif5-10* (Fig EV2A and B). *pif4-2 pif5-10* double mutants showed a stronger stay-green phenotype than the respective single mutants under C-deprivation (Fig EV2A and B). In the *abs3-1D* background, although the progression of senescence in *pif4-2 abs3-1D* was overall similar to that of *abs3-1D*, *pif4-2 pif5-10 abs3-1D* triple mutants showed further delayed senescence compared with *pif5-10 abs3-1D* under C-deprivation (Fig EV2C and D). These observations suggest that both PIF5 and PIF4 are required and share redundant functions in the ABS3-mediated senescence pathway but the role of PIF5 is more prominent.

PIFs regulate diverse plant developmental processes, including hypocotyl elongation and senescence, at least partially through interactions with other TFs (Hornitschek *et al*, 2012; Leivar & Monte, 2014; Pfeiffer *et al*, 2014; Sakuraba *et al*, 2014; Song *et al*, 2014; Zhang *et al*, 2015; Paik *et al*, 2017; Pham *et al*, 2018). Given the close functional link between ARF2 and PIF5/4, we next tested if both PIF5 and PIF4 interact directly with ARF2. In yeast two-hybrid assays, co-expression of BD-ARF2 with AD-PIF5 or AD-PIF4 was capable of activating reporter genes (Figs 3A and EV3A). In bimolecular fluorescence complementation (BiFC) assays, we fused N-terminus and C-terminus of YFP (YN and YC) to ARF2 and PIF5, respectively, and the two fusion proteins, YN-ARF2 and PIF5-YC, were co-expressed transiently in *Arabidopsis* leaf mesophyll protoplasts. Strong YFP signals were reconstituted in the nuclei of cells co-expressing YN-ARF2 and PIF5-YC (Fig 3B). Similarly, co-expression of YN-ARF2 and PIF4-YC also yielded nuclear localized YFP signals (Fig EV3B). Next, we verified the ARF2-PIF5/4 interaction with the *in vitro* pull-down assay. Recombinant PIF5 or PIF4 with a N-terminal maltose-binding protein (MBP) tag and a C-terminal His tag (MBP-PIF5-His or MBP-PIF4-His) was incubated with glutathione S-transferase (GST)-tagged ARF2 (GST-ARF2) and glutathione beads. GST-ARF2 was able to pull down either MBP-PIF5-His or MBP-PIF4-His, whereas MBP-PIF5-His or MBP-PIF4-His was not detected in the pull-down fraction when incubated with GST alone, nor did we found interaction between MBP-His with GST-ARF2 in control assays (Figs 3C and EV3C). Furthermore, we co-expressed hemagglutinin (HA)-tagged ARF2 (ARF2-HA) together with PIF5-GFP, PIF4-GFP, or GFP in protoplasts, and carried out co-immunoprecipitation (IP) assays using GFP-trap. To increase the stable accumulation of PIFs, protoplasts from leaf mesophyll cells of a loss-of-function *phyB* mutant, *phyB-101*, were used (Shen *et al*, 2007; Wang *et al*, 2015a). ARF2-HA was detected in the immunoprecipitated fraction together with PIF5-GFP or PIF4-GFP, but not with GFP alone (Figs 3D and EV3D). These findings uncover previously unknown physical interactions between PIF5/4 and ARF2 proteins.

Finally, to determine the regions of interaction between PIF5 and ARF2, we performed BiFC assays with truncated forms of ARF2 and PIF5. ARF2 has an N-terminal DNA-binding domain (ARF2-N), a middle region (ARF2-M), and a C-terminal dimerization domain (ARF2-C; Appendix Fig S2A; Tiwari *et al*, 2003). N- and C-terminal regions of PIF5 (PIF5-N and PIF5-C) contain the active phyB binding (APB) motif and the DNA-binding bHLH motif, respectively (Appendix Fig S2A; Pedmale *et al*, 2016). Co-expressing YN-ARF2-N or YN-ARF2-M with full-length PIF5-YC reconstituted nuclear localized YFP signals, whereas we did not detect interaction between PIF5-YC and YN-ARF2-C (Appendix Fig S2B). PIF5-N-YC also interacted with YN-ARF2, YN-ARF2-N, and YN-ARF2-M in the nucleus, respectively (Appendix Fig S2B). On the other hand, when PIF5-C-YC was co-expressed with YN-ARF2 or YN-ARF2-N, we observed reconstituted YFP signals that were outside of the nucleus (Appendix Fig S2B). These findings suggest that the N-terminal of PIF5 can interact with the N-terminal and middle region of ARF2 in the nucleus.

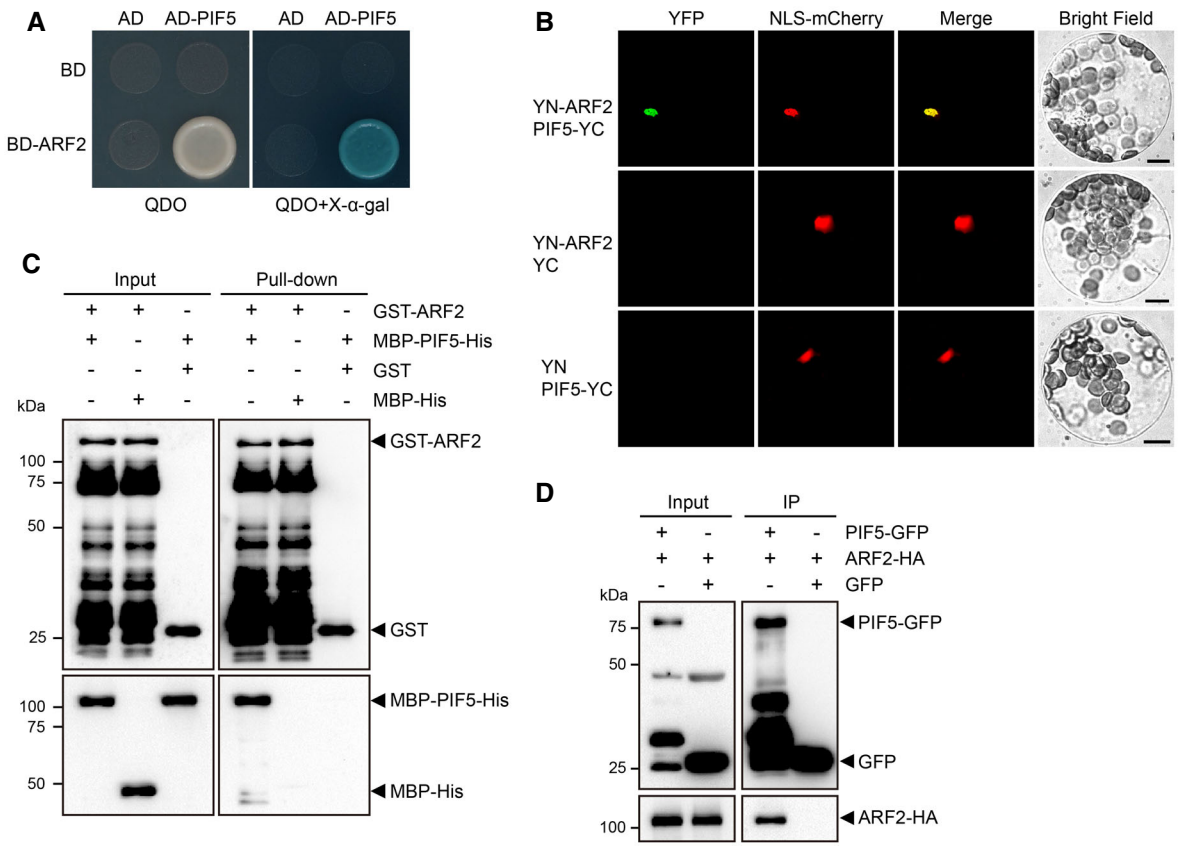

Figure 3. PIF5 interacts directly with ARF2.

A Interaction between ARF2 and PIF5 in the yeast two-hybrid assay. Growth of yeast cells co-transformed with indicated BD and AD vectors was monitored on quadruple dropout medium (QDO, SD-Ade/-His/—Leu/—Trp) and QDO medium containing X-α-gal.

B Interaction between ARF2 and PIF5 in protoplast BiFC assays. YN-ARF2 and PIF5-YC were coexpressed with the nuclear marker NLS-mCherry in *Arabidopsis* mesophyll protoplasts. Coexpression of YN-ARF2 and YC alone or YN alone with PIF5-YC served as negative controls. Bars, 10 μm.

C Direct interaction between GST-ARF2 and MBP-PIF5-His in *in vitro* GST pull-down assays.

D Co-immunoprecipitation of ARF2-HA with PIF5-GFP *in vivo*. ARF2-HA was coexpressed with PIF5-GFP or GFP alone in protoplasts. Proteins co-immunoprecipitated by GFP-Trap beads were immunoblotted with anti-GFP and anti-HA antibodies.

Source data are available online for this figure.

ARF2 and PIF5 regulate senescence interdependently and independently

The physical interaction between ARF2 and PIF5 promoted us to test their functional relationship in regulating senescence. First, we generated overexpression (OE) lines for *ARF2* and *PIF5* by introducing endogenous promoter-driven *pARF2:ARF2-GFP* and *pPIF5:PIF5-GFP* into the WT background, respectively. Multiple independent *ARF2-GFP* OE lines showed significantly increased *ARF2* transcripts and markedly accelerated senescence under C-deprivation and natural growth conditions (Fig 4A–C; Appendix Fig S3A and B). These findings establish that ARF2 is sufficient to promote senescence when overexpressed. Similarly, the overexpression of *PIF5* led to accelerated C-deprivation-induced and natural senescence (Fig 4D–F; Appendix Fig S3C), consistent with previous reports (Sakuraba *et al*, 2014; Song *et al*, 2014; Zhang *et al*, 2015).

Next, *pARF2:ARF2-GFP* OE lines in the WT background (OE-3 and OE-7) were crossed into *pif5-10* (*pif5-10 pARF2:ARF2-GFP*) and *pif4-2 pif5-10* backgrounds (*pif4-2 pif5-10 pARF2:ARF2-GFP*), respectively. Senescence phenotypes of *pARF2:ARF2-GFP* in the WT, *pif5-10*, and *pif4-2 pif5-10* mutant backgrounds under C-deprivation and natural senescence conditions were compared. When *PIF5* is mutated, the ability of *ARF2* overexpression to promote senescence was attenuated in *pif5-10 pARF2:ARF2-GFP* lines (Fig EV4A–D; Appendix Fig S3A). Simultaneous loss of *PIF4* and *PIF5* further delayed the senescence of *ARF2-GFP* OEs under C-deprivation and natural senescence conditions (Fig 4A–C; Appendix Fig S3B). We also crossed two *pPIF5:PIF5-GFP* OEs (OE-2 and OE-20) into the *arf2-20* background (*arf2-20 pPIF5:PIF5-GFP*). The progression of C-deprivation-induced or natural senescence was delayed in *arf2-20 pPIF5:PIF5-GFP* lines compared with *pPIF5:PIF5-GFP* OEs in the WT background, despite similarly elevated *PIF5* transcript levels (Fig 4D–F; Appendix Fig S3C). These data suggest an interdependency of ARF2 and PIF5 in promoting senescence.

On the other hand, *arf2-20 pif5-10* double mutants displayed further delayed senescence and stronger suppression of the accelerated senescence phenotype of *abs3-1D*, compared with the respective single mutants (Fig 4G–J). In line with the finding of non-overlapping

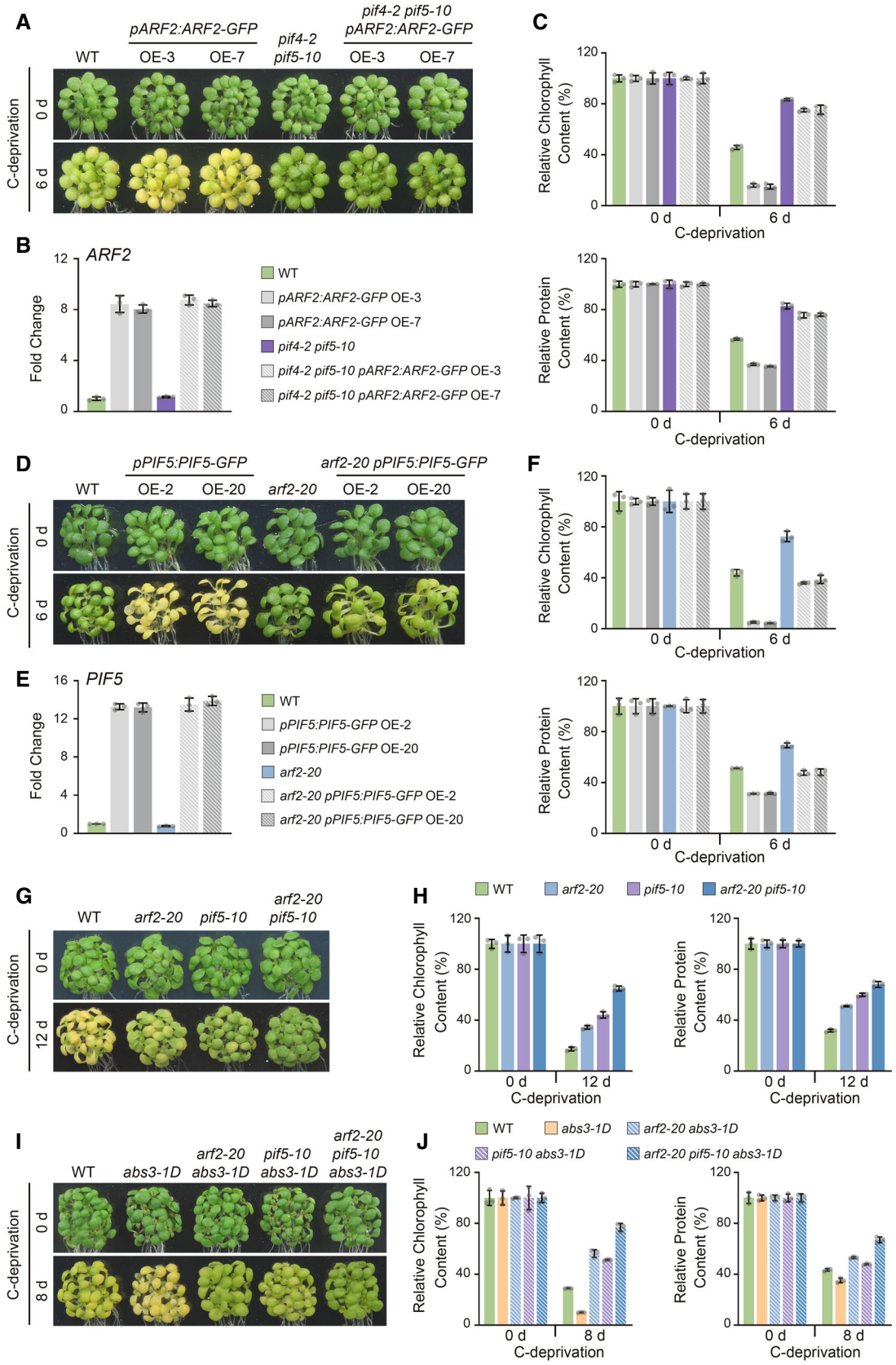

Figure 4.

Figure 4. ARF2 and PIF5 regulate senescence interdependently and independently.

A Seedlings of WT, *pARF2:ARF2-GFP* OEs in the WT background, *pif4-2 pif5-10*, and *pARF2:ARF2-GFP* OEs in the *pif4-2 pif5-10* background before and after 6 days C-deprivation.

B RT-qPCR analysis of *ARF2* expression levels in 7-day-old seedlings of the same genotypes as shown in (A). Fold changes were calculated with respect to the expression level in the WT.

C Chlorophyll and total cellular protein content reduction in genotypes shown in (A) after 6 days C-deprivation. Color legends in (C) are the same as in (B).

D Seedlings of WT, *pPIF5:PIF5-GFP* OEs in the WT background, *arf2-20*, and *pPIF5:PIF5-GFP* OEs in the *arf2-20* background before and after 6 days C-deprivation.

E RT-qPCR analysis of *PIF5* expression levels in 7-day-old seedlings of the same genotypes as shown in (D). Fold changes were calculated with respect to the expression level in the WT.

F Chlorophyll and total cellular protein content reduction in genotypes shown in (D) after 6 days C-deprivation. Color legends in (F) are the same as in (E).

G Seedlings of WT, *arf2-20*, *pif5-10*, and *arf2-20 pif5-10* before and after 12 days C-deprivation.

H Chlorophyll and total cellular protein content reduction in genotypes shown in (G) after 12 days C-deprivation.

I Seedlings of WT, *abs3-1D*, *arf2-20 abs3-1D*, *pif5-10 abs3-1D*, and *arf2-20 pif5-10 abs3-1D* before and after 8 days C-deprivation.

J Chlorophyll and total cellular protein content reduction in genotypes shown in (I) after 8 days C-deprivation.

Data information: In B, C, E, F, H, and J, data are means ± s.d. of three biological replicates.

genes regulated by ARF2 or PIF5 under C-deprivation in RNA-seq analysis (Fig 2E), the genetic interaction between *arf2-20* and *pif5-10* suggests that ARF2 and PIF5 also regulate senescence through pathways that are independent of one another.

ORE1 and *SGR1* are common target genes of ARF2 and PIF5 in the ABS3-mediated senescence pathway

The functional interdependency and the physical interaction between ARF2 and PIF5 suggest they may share common target genes in the ABS3-mediated senescence pathway. To uncover potential common target genes of ARF2 and PIF5, we first carried out bioinformatics analysis based on published DAP-seq data for ARF2 and ChIP-seq data for PIF5 and PIF4 (O'Malley *et al*, 2016; Jin *et al*, 2017). Among the 3,448 ARF2-regulated genes in the *abs3-1D* background, 1,100 were identified in DAP-seq as potential direct targets of ARF2 (Fig 5A; Dataset EV5). Based on published ChIP-seq data, 905 genes of the PIF5-regulated genes in the *abs3-1D* background were identified as potential direct targets of PIF5 and/or PIF4 using the plant transcription factor database (PlantTFDB, http://planttfdb.gao-lab.org/aboutus.php; Fig 5A; Dataset EV5; Jin *et al*, 2017). An overlap of 182 genes, including key senescence promoting-genes *ORE1* and *SGR1*, were found to be putative common target genes of ARF2 and PIF5/4 (Fig 5A). The core sequence (5′-TGTC-3′) for the ARF2-binding motif was identified in the promoters of *ORE1* and *SGR1* in close proximity to the PIF5-binding G-box (Fig 5B).

Second, we examined the direct binding of ARF2 and PIF5 to the same region in promoters of *ORE1* and *SGR1* with ChIP-qPCRs. In transgenic lines expressing *pARF2:ARF2-GFP* or *pPIF5:PIF5-GFP* in the WT background, *ORE1* and *SGR1* promoter sequences were significantly enriched in ChIP fractions compared with those in inputs (Fig 5C and E). Consistently, activated expressions of *ORE1* and *SGR1* under C-deprivation were observed (Fig 5D and F).

Third, given the direct interaction between ARF2 and PIF5, we investigated whether ARF2 and PIF5 require each other to regulate target genes. We performed ChIP-qPCR and RT-qPCR analyses using *pARF2:ARF2-GFP* OE lines in the *pif4-2 pif5-10* background. Interestingly, the binding of ARF2 to the promoters of *ORE1* and *SGR1* was overall similar in *pif4-2 pif5-10* compared with that in the WT background (Fig 5C). However, the induction of *ORE1* and *SGR1* expressions by the overexpression of *ARF2* was greatly compromised (Fig 5D). These findings suggest that ARF2 binds to the promoters of *ORE1* and *SGR1* in a PIF5/4-independent manner but the effect of *ARF2* overexpression on these target genes requires PIF5/4 (Fig 5D).

Next, we performed ChIP-qPCR and RT-qPCR analyses using *pPIF5:PIF5-GFP* OE lines in the *arf2-20* background. The binding of PIF5 to the promoters of *ORE1* and *SGR1* and the activated

Figure 5. *ORE1* and *SGR1* are common target genes of ARF2 and PIF5 in the ABS3-mediated senescence pathway.

A The venn diagram of putative ARF2 target genes and PIF5/4 target genes.

B Diagrams of the promoter regions of *ORE1* and *SGR1*. Orange arrow heads indicate the positions of G-box and purple arrow heads indicate the positions of the core sequence (5′-TGTC-3′) for ARF2 binding. Horizontal lines indicate fragments amplified in ChIP-qPCRs.

C ChIP-qPCR analysis of ARF2-GFP binding to the promoters of *ORE1* and *SGR1* in the WT and *pif4-2 pif5-10* backgrounds.

D RT-qPCR analysis of *ORE1* and *SGR1* expression levels in seedlings of WT, *pARF2:ARF2-GFP* OEs in the WT background, *pif4-2 pif5-10*, and *pARF2:ARF2-GFP* OEs in the *pif4-2 pif5-10* background before and after 4 days C-deprivation. Fold changes were calculated with respect to the expression level in the WT before C-deprivation.

E ChIP-qPCR analysis of PIF5-GFP binding to the promoters of *ORE1* and *SGR1* in the WT and *arf2-20* backgrounds.

F RT-qPCR analysis of *ORE1* and *SGR1* expression levels in seedlings of WT, *pPIF5:PIF5-GFP* OEs in the WT background, *arf2-20*, and *pPIF5:PIF5-GFP* OEs in the *arf2-20* background before and after 4 days C-deprivation. Fold changes were calculated as in (D).

G Hypocotyl elongation in seedlings of WT, *pPIF5:PIF5-GFP* OEs in the WT background, *arf2-20*, and *pPIF5:PIF5-GFP* OEs in the *arf2-20* background. Seedlings were grown under continuous light for 1 week.

H RT-qPCR analysis of *PIL1* and *YUC8* expression levels in seedlings shown in (G). Fold changes were calculated with respect to the expression level in the WT. Color legends in (H) are the same as in (F).

I Diagrams of the promoter regions of *PIL1* and *YUC8*. Orange arrow heads indicate the positions of G-box. Horizontal lines indicate fragments amplified in ChIP-qPCRs.

J ChIP-qPCR analysis of PIF5 binding to the promoters of *PIL1* and *YUC8* in the WT and *arf2-20* backgrounds.

Data information: In D, F, and H, data are means ± s.d. of three biological replicates. In C, E, and J, fold enrichments were calculated with respect to the input. *PP2A* served as a non-binding control. Data are means ± s.d. of three technical replicates. Two-tailed *t* test, n.s., not significant, ****$P < 0.0001$. The experiment has been independently repeated with similar results.

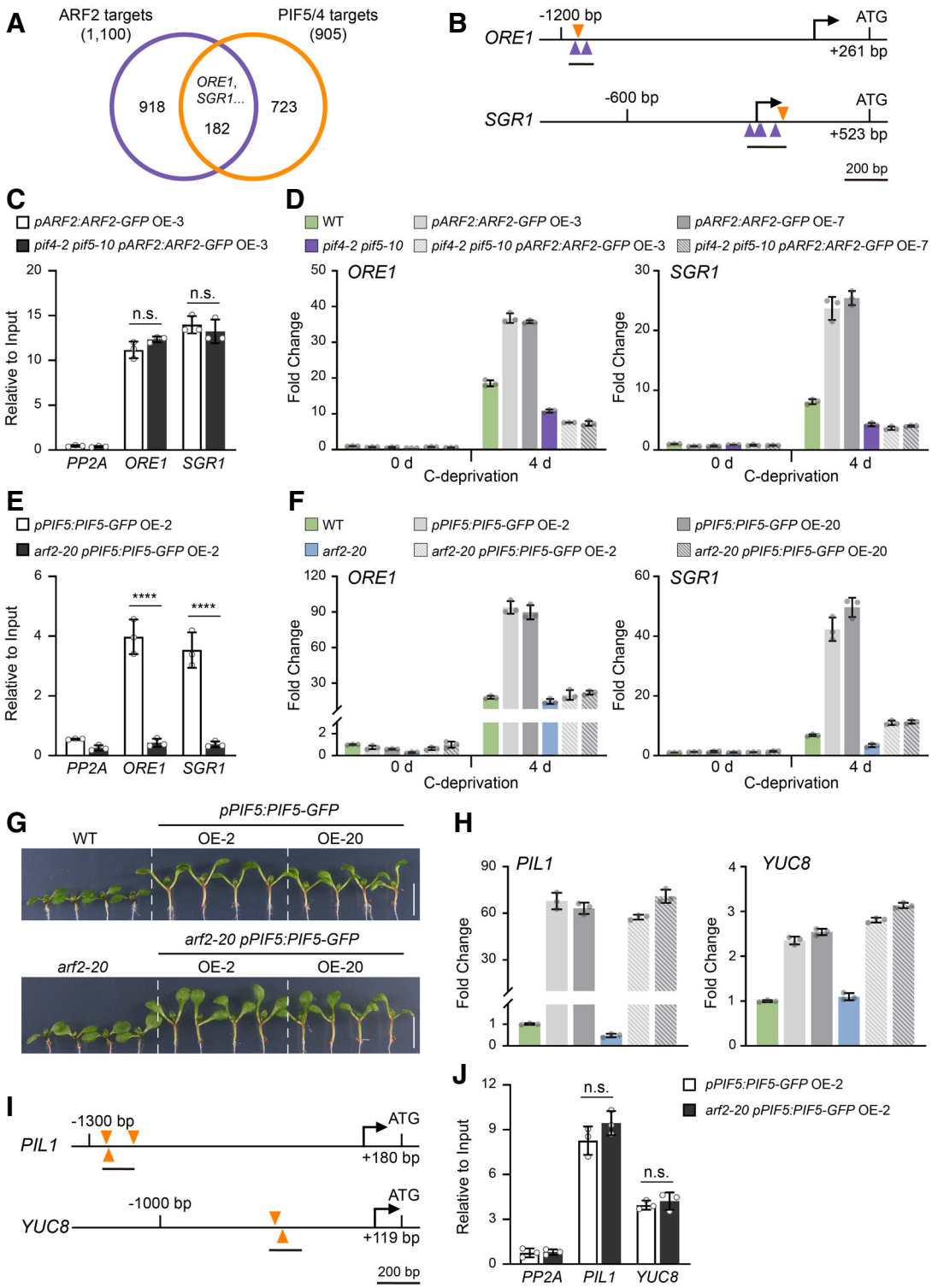

Figure 5.

expressions of *ORE1* and *SGR1* by *PIF5* overexpression were significantly reduced in the *arf2-20* background compared with those in the WT background (Fig 5E and F). In stark contrast, the promotion of cell elongation by PIF5 was not affected by the loss of *ARF2*. Light-grown *arf2-20 pPIF5:PIF5-GFP* seedlings displayed the distinctive elongated hypocotyl and petiole phenotype characteristic of the overexpression of *PIF5* (Fig 5G; Appendix Fig S3D). Consistently, the binding of PIF5 to its known targets involved in promoting cell elongation, such as *PIF3-LIKE 1* (*PIL1*) and *YUCCA 8* (*YUC8*) and the activation of *PIL1* and *YUC8* expression were similar in *pPIF5:PIF5-GFP* lines in WT and *arf2-20* backgrounds (Fig 5H–J). These data demonstrate that PIF5 binds to the promoters of *ORE1* and *SGR1* in

an ARF2-dependent manner and requires ARF2 to reach full induction of *ORE1* and *SGR1*.

Finally, if the induction of *ORE1* and *SGR1* is a direct output of the ARF2-PIF5 functional module, a loss-of-function mutation of *ORE1* or *SGR1* would be expected to suppress the premature senescence of *abs3-1D*. To test this, we obtained a T-DNA insertion allele of *ORE1*, designated *ore1-101* (SAIL_694_C04), and generated a knockout allele of *SGR1*, *sgr1-101*, using the CRISPR-Cas9 technology (Appendix Fig S4A and B). Both *ore1-101* and *sgr1-101* suppressed the premature senescence phenotype of *abs3-1D* under C-deprivation (Fig EV5A–H). Furthermore, the overexpression of *ORE1* and *SGR1* in the *mateq* background markedly accelerated senescence of *mateq* under C-deprivation (Fig EV5I–N). These data suggest that the *ORE1* and *SGR1* are common target genes of ARF2 and PIF5 in the ABS3-mediated senescence pathway.

The promotion of senescence by ARF2 and PIF5 requires the ABS3 subfamily MATEs

Our suppressor analysis indicate that ARF2 and PIF5 are required in the ABS3-mediated senescence pathway. To determine if the promotion of senescence by ARF2 and PIF5 also requires the ABS3 subfamily MATEs, we overexpressed *pARF2:ARF2-GFP* and *pPIF5:PIF5-GFP* in *mateq*, the quadruple loss-of-function mutants of four *ABS3* subfamily genes (Jia *et al*, 2019), respectively. The expression levels of *ARF2* and *PIF5* in the overexpression lines were determined with RT-qPCR, and *ARF2* and *PIF5* overexpression lines with comparable expression levels in WT and *mateq* backgrounds were selected for further analysis (Fig 6A and B). In the WT background, overexpression of either *pARF2:ARF2-GFP* or *pPIF5:PIF5-GFP* resulted in significantly aggravated senescence under C-deprivation (Fig 6C–F). In contrast, *pARF2:ARF2-GFP* OEs in the *mateq* background showed significantly slowed senescence compared with *pARF2:ARF2-GFP* OEs in the WT background under C-deprivation (Fig 6C and E). Similar to the findings with *pARF2:ARF2-GFP* OEs, the accelerated senescence caused by the overexpression of *pPIF5:PIF5-GFP* was also abolished in the *mateq* background under C-deprivation (Fig 6D and F). The induction of *ORE1* and *SGR1*, direct targets of ARF2 and PIF5, was also compromised in *mateq pARF2:ARF2-GFP* and *mateq pPIF5:PIF5-GFP* under C-deprivation (Fig 6G and H). Interestingly, the *mateq* background did not impact the capability of PIF5 to activate its direct targets, *PIL1* and *YUC8*, in the cell elongation pathway (Fig 6I). In natural senescence, both *pARF2:ARF2-GFP* and *pPIF5:PIF5-GFP* OEs also showed lesser degrees of senescence in the *mateq* background than in the WT background (Appendix Fig S5A and B). These data suggest that the abilities of ARF2 and PIF5 to promote senescence are also partially dependent on the ABS3 subfamily MATEs, further supporting the functional links between ARF2, PIF5, and MATEs in regulating senescence.

Feedback transcriptional repression of *ABS3* by ARF2

During our RT-qPCR and RNA-seq analyses, we consistently observed that the accumulation of *ABS3* transcripts was significantly elevated in the *arf2-20* background but not in the *pif5-10* background, suggesting that ARF2 may be able to negatively regulate the transcription of *ABS3* (Fig 1C and D). Interestingly, the binding of ARF2 to the *ABS3* promoter was also identified in ARF2 DAP-seq (O'Malley *et al*, 2016). Thus, we investigated whether ARF2 binds directly to the *ABS3* promoter and represses *ABS3* expression. Multiple potential ARF family TF binding core sequences (5′-TGTC-3′) were identified in the *ABS3* promoter (Fig 7A). ChIP-qPCR using *pARF2:ARF2-GFP* OE lines revealed the enrichment of ARF2 binding to multiple regions in the *ABS3* promoter (Fig 7B). To narrow down the potential ARF2-binding region in the *ABS3* promoter, mutant forms of the *ABS3* promoter with deletions of regions harboring the core ARF2-binding sequence (5′-TGTC-3′), $pABS3^{\Delta R1}$, $pABS3^{\Delta R2}$, $pABS3^{\Delta R3}$, and $pABS3^{\Delta R4}$, were generated, respectively (Fig 7A). Wild-type and mutant forms of *pABS3:GFP* reporters were co-expressed with *p35S:ARF2-HA* in protoplasts. The repression of *GFP* expression by ARF2-HA was abolished only when $pABS3^{\Delta R2}$*:GFP* was co-expressed (Fig 7C and D; Appendix Fig S6). There are two putative ARF2-binding sites (5′-TGTC-3′), S1 and S2, in the R2 region (Fig 7A). To further dissect the roles of S1 and S2, two additional mutant *pABS3-GFP* reporter constructs, $pABS3^{\Delta S1}$*:GFP* and $pABS3^{\Delta S2}$*:GFP*, in which the S1 and S2 sites were deleted, respectively, were generated. We found that the repression of *GFP* expression by ARF2-HA was abolished in $pABS3^{\Delta S2}$*:GFP*, but not in $pABS3^{\Delta S1}$*:GFP* (Fig 7C and D; Appendix Fig S6). These data suggest that ARF2 represses *ABS3* expression through direct binding to the *ABS3* promoter and the S2 site is likely required for ARF2 to repress *ABS3* expression. Notably, the repression of *ABS3* expression by ARF2 is independent of PIF5 and PIF4, as we also detected decreased *ABS3* transcript levels in *pif4-2 pif5-10 pARF2:ARF2-GFP* OEs (Fig 7E). Together, these findings suggest a negative feedback regulation scheme of *ABS3* by ARF2, in which increased expressions

Figure 6. ABS3 subfamily MATEs are required for ARF2 and PIF5 to promote senescence.

A RT-qPCR analysis of *ARF2* expression levels in 7-day-old seedlings of WT, *pARF2:ARF2-GFP* OEs in the WT background, *mateq*, and *pARF2:ARF2-GFP* OEs in the *mateq* background. Fold changes were calculated with respect to the expression level in the WT.

B RT-qPCR analysis of *PIF5* expression levels in 7-day-old seedlings of WT, *pPIF5:PIF5-GFP* OEs in the WT background, *mateq*, and *pPIF5:PIF5-GFP* OEs in the *mateq* background. Fold changes were calculated as in (A).

C Seedlings of the same genotypes as in (A) before and after 6 days and 9 days C-deprivation.

D Seedlings of the same genotypes as in (B) before and after 6 days and 11 days C-deprivation.

E, F Chlorophyll and total cellular protein content reduction in genotypes shown in A (E) after 6 days and 9 days C-deprivation and in genotypes shown in B (F) after 6 days and 11 days C-deprivation.

G, H RT-qPCR analysis of *ORE1* and *SGR1* expression levels in genotypes shown in A (G) and B (H) before and after 4 days C-deprivation. Fold changes were calculated with respect to the expression level in the WT before C-deprivation.

I RT-qPCR analysis of *PIL1* and *YUC8* expression levels in 7-day-old seedlings of the same genotypes as shown in (B). Fold changes were calculated as in (A).

Data information: Color legends in (E) and (G) are the same as in (A). Color legends in (F), (H), and (I) are the same as in (B). In A, B, and E-I, data are means ± s.d. of three biological replicates.

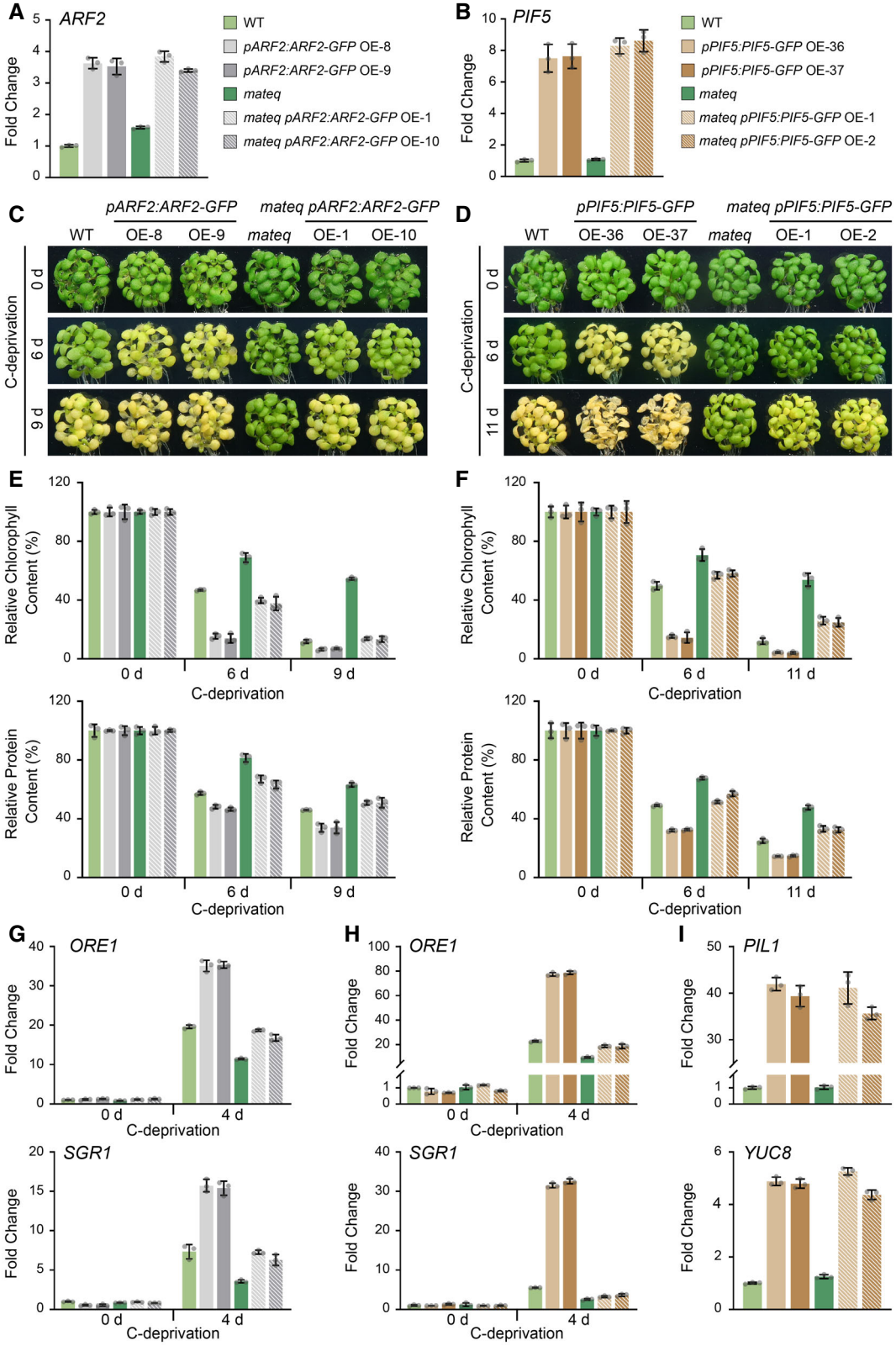

Figure 6.

of *ABS3* promote senescence via the ARF2-PIF5 mediated transcriptional regulation, while the transcription of *ABS3* itself is directly repressed by ARF2.

Discussion

Through large-scale genetic suppressor analysis, we showed that mutations in two transcription factor genes, *ARF2* and *PIF5*, respectively, can effectively suppress the early senescence phenotype of *abs3-1D* under C-deprivation and natural senescence conditions (Figs 1 and EV1; Appendix Fig S1). More importantly, the elevated expressions of *SAGs*, such as *ORE1* and *SGR1*, were also mitigated in *abs3-1D* upon the mutation of *ARF2* or *PIF5* (Fig 1). Moreover, the global transcriptional reprogramming caused by the elevated expression of *ABS3* in *abs3-1D* under C-deprivation, was largely dependent on ARF2 and PIF5, as revealed in RNA-seq analysis (Fig 2). These results suggest that ARF2 and PIF5 act as signaling components responsible for the transcriptional responses in the ABS3-mediated senescence pathway (Fig 7F). ARF2 belongs to the plant ARF family TFs which are important components of the auxin signaling pathway (Okushima *et al*, 2005). Surprisingly, ARF2 was identified in multiple forward genetic screens and implicated in a large spectrum of processes in *Arabidopsis*, suggesting that it may possess additional functions beyond a typical ARF protein (Li *et al*, 2004; Schruff *et al*, 2006; Lim *et al*, 2010; Zhao *et al*, 2016). *ARF2* is involved in the regulation of flowering time, fertility, seed size, photomorphogenesis, abscisic acid signaling, and low K^+ responses (Li *et al*, 2004; Ellis *et al*, 2005; Schruff *et al*, 2006; Wang *et al*, 2011; Richter *et al*, 2013; Zhao *et al*, 2016). Supporting the genetic evidence that ARF2 may function beyond the auxin signaling pathway, microarray data indicate that auxin-regulated gene expression was largely unaffected in *arf2* mutants (Ellis *et al*, 2005). Instead, *ACC SYNTHASE* (*ACS*) genes are down-regulated in *arf2*, suggesting ARF2 plays a positive role in regulating the biosynthesis of ethylene that promotes leaf senescence (Okushima *et al*, 2005). *ARF2* was also identified as *ORE14* in genetic screens for mutants with delayed *SAG* expression and several studies have reported that *arf2* mutants showed a marked delay of leaf senescence (Ellis *et al*, 2005; Okushima *et al*, 2005; Lim *et al*, 2010). However, previous efforts and our own attempts with 35S promoter-driven *ARF2* overexpression gave rise to loss-of-function *arf2* phenotypes, probably due to co-suppression (Okushima *et al*, 2005). In this work, we showed that the loss of *ARF2* genetically suppressed the accelerated senescence of the *abs3-1D* mutant (Fig 1A, C, E, G and I), while the overexpression of endogenous promoter-driven *ARF2* leads to an accelerated senescence phenotype (Fig 4A–C), clearly demonstrating ARF2 as a positive regulator of plant senescence.

PIF5 belongs to a subfamily of bHLH family of TFs that also includes PIF4 and PIF3 in *Arabidopsis* (Leivar *et al*, 2008b). PIFs are central signaling hubs in various developmental processes including photomorphogenesis, thermomorphogenesis, shade avoidance, phototropism, and circadian clock regulation (Lorrain *et al*, 2008; Leivar *et al*, 2008b; Keller *et al*, 2011; Hornitschek *et al*, 2012; Li *et al*, 2012; Leivar & Monte, 2014; Pfeiffer *et al*, 2014; Sakuraba *et al*, 2014; Song *et al*, 2014; Zhang *et al*, 2015; Pedmale *et al*, 2016; Paik *et al*, 2017; Shor *et al*, 2017; Pham *et al*, 2018). The regulation of these processes is underpinned by a large complement of PIF5 direct target genes (Hornitschek *et al*, 2012; Sakuraba *et al*, 2014; Song *et al*, 2014, 2018; Zhang *et al*, 2015; Pedmale *et al*, 2016; Shor *et al*, 2017). In shade avoidance response, PIF5, PIF4, and PIF7 directly activate auxin biosynthesis genes, such as *YUCCAs* (*YUCs*) to promote hypocotyl elongation (Lorrain *et al*, 2008; Keller *et al*, 2011; Li *et al*, 2012). PIF5 and PIF4 also interact with blue light receptor CRY2 to promote phototropic growth (Pedmale *et al*, 2016). In addition, PIF5, PIF4, and PIF3 have been reported to regulate senescence (Sakuraba *et al*, 2014; Song *et al*, 2014; Zhang *et al*, 2015). Senescence promoting genes, such as *ORE1* and *SGR1*, are direct targets of PIF5 and PIF4 (Sakuraba *et al*, 2014; Song *et al*, 2014; Liebsch & Keech, 2016; Woo *et al*, 2019). However, additional components in the PIF-regulated senescence pathway remain largely unexplored. Here we show that PIF5 and PIF4 act redundantly to promote senescence in the ABS3-mediated senescence pathway (Figs 1B, D, F, H, and J, and EV2).

One key discovery we demonstrated in this work is that ARF2 and PIF5/4 work in concert to promote senescence in plants (Fig 7F). We uncovered a previously unknown physical interaction between ARF2 and PIF5/4 (Figs 3 and EV3) and provided evidence supporting that a close functional interdependency between ARF2 and PIF5/4 in promoting senescence in both C-deprivation and natural senescence processes (Fig 4A–F; Appendix Fig S3). First, our RNA-seq data and bioinformatics analyses showed significant overlapping between ARF2- and PIF5- regulated genes under C-deprivation and identified putative common target genes of ARF2 and PIF5 (Figs 2E and 5A). Next, we showed that ARF2 and PIF5 can bind to the promoters of their common targets *ORE1* and *SGR1* (Fig 5B, C and E). Third, ARF2 and PIF5 require each other to induce the expression of *ORE1* and *SGR1* and to promote senescence (Fig 5D and F). Interestingly, the modes of functional dependency between ARF2 and PIF5 were different. Without PIF5/4, ARF2 was

Figure 7. Feedback transcriptional repression of *ABS3* by ARF2.

A A diagram of the promoter region of *ABS3*. Purple arrow heads indicate the positions of the core sequence (5′-TGTC-3′) for ARF2 binding. Horizontal lines indicate the fragments amplified in ChIP-qPCRs. Brackets indicate the deleted regions in *pABS3*$^{\Delta R1}$, *pABS3*$^{\Delta R2}$, *pABS3*$^{\Delta R3}$, and *pABS3*$^{\Delta R4}$, respectively.

B ChIP-qPCR analysis of ARF2-GFP binding to the promoter of *ABS3*. Fold enrichments were calculated with respect to the input. *PP2A* served as a non-binding control. Data are means ± s.d. of four technical replicates. The experiment has been independently repeated three times with similar results.

C *pABS3:GFP* or *pABS3*$^{\Delta S2}$*:GFP* was expressed in WT mesophyll protoplasts with or without *p35S:ARF2-HA*. *p35S:mCherry* was co-transfected and served as a transfection control. Protoplasts were examined with fluorescence microscopy. Experiments were independently repeated three times with similar results. Bars, 100 μm.

D Dot plots of GFP relative fluorescence intensity in protoplasts expressing WT and mutant forms of *pABS3:GFP* with or without *p35S:ARF2-HA*. Data are median with interquartile range, *n* is indicated in parentheses, two-tailed Mann–Whitney test, n.s., not significant, ****$P < 0.0001$.

E RT-qPCR analysis of *ABS3* expression levels in 7-day-old seedlings of WT, *pARF2:ARF2-GFP* OEs in the WT background, *pif4-2 pif5-10*, and *pARF2:ARF2-GFP* OEs in the *pif4-2 pif5-10* background. Fold changes were calculated with respect to the expression level in the WT. Data are means ± s.d. of three biological replicates.

F A working model depicting the ARF2-PIF5/4 functional module in the ABS3-mediated senescence pathway.

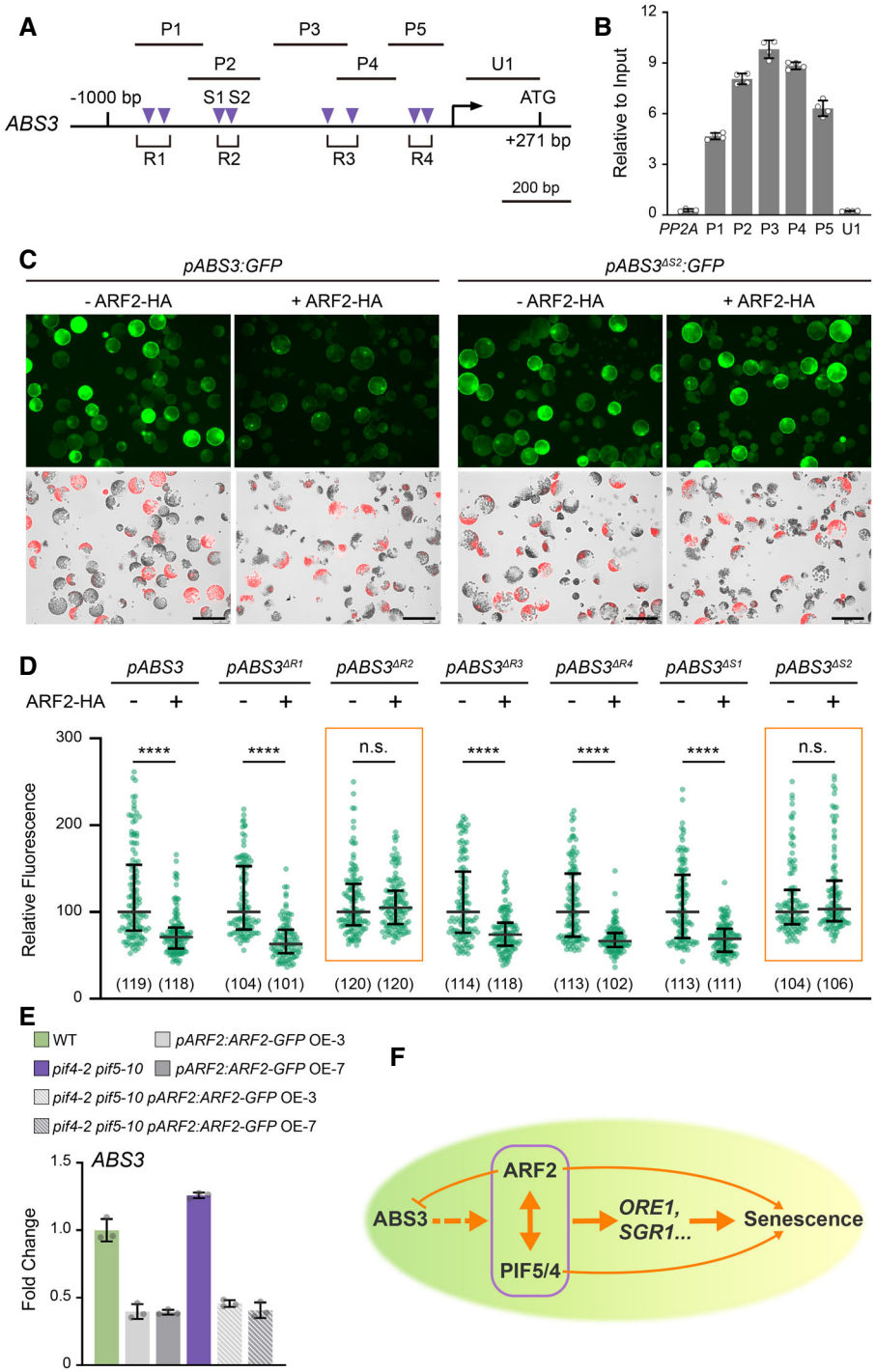

Figure 7.

still capable of binding the promoters of *ORE1* and *SGR1* but the induction of their expressions was attenuated under C-deprivation (Fig 5C and D). In contrast, when *ARF2* was mutated, the ability of PIF5 to bind to the promoters of *ORE1* and *SGR1* and activate their expressions was compromised (Fig 5E and F). In addition, ARF2 and PIF5 likely also regulate senescence independently. First, in our RNA-seq analysis, we found that ARF2 and PIF5 regulate non-overlapping genes under C-deprivation as well (Fig 2E). Next, bioinformatics analysis also identified non-overlapping putative target genes for ARF2 and PIF5 (Fig 5A). Last, the senescence phenotype of *arf2-20 pif5-10* double mutants is consistent with independent functions of ARF2 and PIF5 (Fig 4G–J).

The functional relationship between ARF2 and PIF5/4 in regulating senescence is reminiscent of the regulation of hypocotyl

elongation by the tripartite interactions between BRASSINAZOLE RESISTANT 1 (BZR1), a key TF in plant hormone brassinosteroid (BR) signaling, PIF4, and ARF6 (Oh *et al*, 2014). ARFs can function as both transcription activators and repressors (Ulmasov *et al*, 1999; Tiwari *et al*, 2003). ARF6 is a transcription activator while ARF2 is thought to be a transcription repressor in auxin signaling (Ulmasov *et al*, 1999; Tiwari *et al*, 2003; Oh *et al*, 2014). Unexpectedly, our findings indicate that ARF2 can promote the expression of *SAGs*, such as *ORE1* and *SGR1*. It is possible that ARF2 may be able to form both transcriptional repressing and transcriptional activating complexes in different processes through interactions with distinct partners. It will be interesting to explore whether additional transcription factors, such as BZR1 and its homolog, BRI1-EMS-SUPPRESSOR 1 (BES1), also participate in the regulation of senescence through interaction with ARF2 and PIF5/4.

Notably, neither the well-established enhanced hypocotyl cell elongation phenotype of *PIF5* OEs nor the binding of PIF5 to its cell elongation targets was affected by the loss of *ARF2* (Fig 5G–J). These findings suggest that the interaction between ARF2 and PIF5 is specific for the regulation of senescence, while other genetic factors might work with PIF5 to facilitate the control of hypocotyl cell elongation. In agreement with this notion, PIF proteins are known to interact with other TFs to regulate diverse cellular processes (Paik *et al*, 2017; Pham *et al*, 2018). Modulating the interaction between PIFs and their interactors may represent a common mechanism for plant cells to differentially regulate PIF activities.

Finally, we discovered reciprocal regulations between ABS3-subfamily MATEs and the ARF2-PIF5/4 functional module (Fig 7F). On one hand, an increased expression of *ABS3* in *abs3-1D* activates the transcription of *SAGs* via TFs ARF2 and PIF5/4, while loss of ABS3 subfamily MATEs dampens the senescence promoting effects of *ARF2* and *PIF5* overexpressions (Fig 6). Since the transcripts levels of *ARF2* and *PIF5* were largely unaffected by the gain- or loss-of function of *ABS3* subfamily *MATEs*, it is possible that ABS3 subfamily MATEs may activate ARF2-PIF5 module to promote senescence through post-transcriptional regulation (Fig 7F). On the other hand, we revealed a direct feedback inhibition of *ABS3* transcription by ARF2, establishing another intriguing layer of regulation in the ABS3-mediated senescence pathway (Fig 7). ARF2 binds directly to the promoter of *ABS3* and represses *ABS3* transcription (Fig 7A–D). Feedback regulation is a common mechanism in biology to fine-tune the output of developmental signals. For example, in plant hormone jasmonic acid-induced senescence pathway, TFs Dof2.1 and MYC2 activate each other's expression thereby forming a senescence-promoting feedforward loop (Zhuo *et al*, 2020). Negative feedback has also been observed in the regulation of plant senescence. In nitrogen deficiency-induced senescence, the protein stability of ORE1 is negatively regulated through protein degradation via an E3 ubiquitin ligase NITROGEN LIMITATION ADAPTATION (NLA; Park *et al*, 2018). In this work, we showed that a negative feedback regulation of *ABS3* by ARF2 operates in the ABS3-mediated senescence pathway, further underlining the complexity of senescence regulation in plants (Fig 7F). It is conceivable that the highly ordered and coordinated nature of plant senescence necessitates multiple layers of regulation including negative feedback mechanisms to ensure robust responses to highly dynamic internal and external cues.

Materials and Methods

Plant materials

All *Arabidopsis* lines used in this study are in the Columbia-0 (Col-0) background. *abs3-1D* and *mateq* (*abs3-1 abs4-1 abs3l1–1 abs3l2–1*) have been described (Wang *et al*, 2015a). T-DNA insertional mutants of *PIF4* (*pif4-2*, SAIL_1288_E07) and *ORE1* (SAIL_694_C04, designated *ore1-101* in this study) were obtained from the *Arabidopsis* Biological Resource Center. *abs3-1D* suppressor lines *FD11-55* (*arf2-20 abs3-1D*) and *FD18-70* (*pif5-10 abs3-1D*) were identified in this study. *arf2-20* and *pif5-10* single mutants were obtained by backcrossing *FD11-55* (*arf2-20 abs3-1D*) and *FD18-70* (*pif5-10 abs3-1D*) with the WT, respectively. The double mutants *arf2-20 pif5-10*, *pif4-2 abs3-1D*, *pif4-2 pif5-10* and triple mutants *arf2-20 pif5-10 abs3-1D*, *pif4-2 pif5-10 abs3-1D* were generated in this study by genetic crossing. The double mutant *sgr1-101 abs3-1D* was generated by the CRISPR-Cas9 technology. Mutant genotypes were validated by PCR and sequencing. Primers used for genotyping are listed in Appendix Table S1. The *arf2-20 pPIF5:PIF5-GFP* lines were generated by crossing two non-segregating *pPIF5:PIF5-GFP* lines in the WT background with *arf2-20*. Similarly, the *pif4-2 pif5-10 pARF2:ARF2-GFP* lines and *pif5-10 pARF2:ARF2-GFP* lines were generated by crossing two non-segregating *pARF2:ARF2-GFP* lines in the WT background with *pif4-2 pif5-10* and *pif5-10*, respectively. The rest of the transgenic lines were generated using the Agrobacterium-mediated floral dip method (Clough & Bent, 1998).

Plant growth conditions

Seeds were surface-sterilized and stratified at 4°C for 2 days in the dark before sowing. Plants were grown under ~80 μmol m^{-2} s^{-1} illumination at 22°C. Plants used in protoplast preparations were grown on peat pellets (Jiffy-7, Jiffy Group) under 12 h/12 h day/night cycle. For all other purposes, plants were grown on commercial soil mix (Pindstrup) under continuous light. C-deprivation treatment was carried out as previously described (Jia *et al*, 2019). Briefly, seeds were sown on 1/2 Murashige and Skoog (MS) medium (M153, PhytoTechnology Laboratories) supplemented with 1% (w/v) Bacto agar (214010, BD) and 1% (w/v) sucrose and allowed to grow for 7 days at 22°C under continuous light. Seedlings were then transferred onto 1/2 MS medium with 1% (w/v) Bacto agar and no sucrose and kept in the dark at 22°C for indicated time periods.

abs3-1D suppressor screen

EMS mutagenesis of *abs3-1D* seeds was carried out as described (Li *et al*, 2021). Briefly, ~ 48,000 homozygous *abs3-1D* seeds were mutagenized and divided into 30 pools, each containing ~1,600 M1 plants. M2 seeds were harvested and used for screening. M2 seeds were grown on 1/2 MS medium supplemented with 1% sucrose for 7 days and then subjected to C-deprivation treatment for 6 days. On each plate, 10 *abs3-1D* seedlings were treated with C-deprivation in parallel with the M2 seedlings. M2 seedlings displayed delayed senescence compared with *abs3-1D* were considered as candidate suppressors, transferred to soil, selfed, and harvested individually. For each pool, ~ 6,000 M2 seeds were screened for the suppression

of the accelerated senescence of *abs3-1D* under C-deprivation. After validating the delayed senescence phenotype in M3 generation, candidate suppressors were backcrossed with WT for two to three rounds to clear their genetic background. Genomic DNA from 20–30 pooled suppressors from the F2 population of a backcross was purified using the DNAquick Plant System kit (4992710, TIANGEN Biotech). DNA library preparation, genome resequencing, reads mapping, and SNP identification were performed at Novogene in Tianjin, China.

Vectors

Primers used in vector construction are listed in Appendix Table S1. Information on vectors generated in this study is provided in Appendix Table S2.

To express ARF2-HA in protoplasts, the coding sequence of *ARF2* was amplified and assembled with PCR amplified backbone of *HBT95-2 × HA* using the NEBbuilder HiFi DNA Assembly Master Mix (New England Biolabs; Yoo *et al*, 2007). To express PIF5-GFP and PIF4-GFP in protoplasts, coding sequences of *PIF5* and *PIF4* were amplified, restriction digested, and cloned into *pUC18-p35S:GFP*. Vectors for expressing YN and YC fusion proteins in protoplasts have been described (Jia *et al*, 2019). For BiFC assays, coding sequences of *ARF2*, *ARF2-N*, *ARF2-M*, and *ARF2-C* were amplified and fused to the C-terminus of YN in *pUC18-p35S:YN* to generate *pUC18-p35S:YN-ARF2*, *pUC18-p35S:YN-ARF2-N*, *pUC18-p35S:YN-ARF2-M*, and *pUC18-p35S:YN-ARF2-C*, respectively. Coding sequences of *PIF5*, *PIF4*, *PIF5-N*, and *PIF5-C* were amplified and fused to the N-terminus of YC in *pUC18-p35S:YC* to generate *pUC18-p35S:PIF5-YC*, *pUC18-p35S:PIF4-YC*, *pUC18-p35S:PIF5-N-YC*, *pUC18-p35S:PIF5-C-YC*, respectively.

For yeast two-hybrid assay, coding sequences of *ARF2*, *PIF5*, and *PIF4* were amplified and cloned into *pGBKT7* (BD vector; 630443, Takara Bio) and *pGADT7* (AD vector; 630442, Takara Bio) to generate *pGBKT7-ARF2*, *pGADT7-PIF5*, and *pGADT7-PIF4*, respectively.

For recombinant protein expression, additional constructs were generated. To express recombinant ARF2 with an N-terminal GST tag (GST-ARF2), the coding sequence of *ARF2* was cloned into *pGEX-4T-1* (27-4580-01, GE Healthcare). To express recombinant PIF5 with an N-terminal MBP and a C-terminal His-tag (MBP-PIF5-His), a *PIF5-His* fusion generated by PCR was assembled with the backbone of *pMAL-c4x* (E8000S, New England Biolabs) using the NEBbuilder HiFi DNA Assembly Master Mix (E2621, New England Biolabs). To express MBP-PIF4-His, coding sequence of *PIF4* was amplified from *pUC18-p35S:PIF4-GFP* and used to replace *PIF5* in *pMAL-c4X-MBP-PIF5-His*.

For protoplast effector/reporter assays, the promoter of *ABS3* was amplified and used to replace *p35S* in *pUC18-p35S:GFP* to generate *pUC18-pABS3:GFP*. To generate mutant forms *pABS3*, fragment flanking the deleted regions were amplified and assembled with the backbone of *pUC18* using the NEBbuilder HiFi DNA Assembly Master Mix (E2621, New England Biolabs).

For plant transformation, genomic regions encompassing the promoter and coding regions of *ARF2*, *PIF5*, *ORE1*, and *SGR1* were amplified and cloned into a binary vector *pCambia1300-GFP* to have GFP fused to the C-termini of ARF2, PIF5, ORE1, and SGR1 respectively. Transgenic lines were screened on 1/2 MS medium supplemented with 0.8% (w/v) agar and 25 mg l^{-1} hygromycin.

To generate knockout mutant of *SGR1* with the CRISPR-Cas9 technology, two sgRNAs that targeted two sites in the coding sequences of *SGR1* were designed using the CRISPRscan (https://www.crisprscan.org/) website (Moreno-Mateos *et al*, 2015). The dual-gRNA cassette was amplified by overlapping PCR using primers SGR1-DT1-F, SGR1-DT1-BsF, SGR1-DT1-R, and SGR1-DT1-BsR and the *pCBC-DT1T2* plasmid as the template. The resulting PCR products were digested with BsaI, and cloned into the *pHEE2A* binary vector (Wang *et al*, 2015b). The resulting *pHEE2A-dual-sgSGR1* vector was used to transform *abs3-1D*. Deletion mutants of *SGR1* were identified in T1 generation by PCR and sequencing.

Chlorophyll and total cellular protein content measurement

To measure chlorophyll and total cellular protein contents of the seedlings before and after C-deprivation treatment, whole seedlings were weighed and ground in liquid nitrogen. Total chlorophyll was extracted with 95% ethanol at 4°C in the dark with gentle agitation overnight. Tissue debris were then removed by centrifugation at 12,000 *g* at 4°C for 10 min. Chlorophyll content (μg/mg fresh tissue weight) in supernatants was determined (Lichtenthaler, 1987). Total protein was extracted with 50 mM Tris–HCl pH 6.8, 2% sodium dodecyl sulfate (SDS), and 10% glycerol at 95°C for 5 min, supernatants were separated from tissue debris by centrifugation at 12,000 *g* at RT for 10 min. Protein contents in supernatants (μg/mg fresh tissue weight) were measured using a Pierce™ Rapid Gold BCA Protein Assay Kit (A53226; Thermo Fisher Scientific) following the manufacturer's instructions. To calculate relative chlorophyll and protein content, chlorophyll and protein content before C-deprivation was defined as 100% in each genotype. Data were generated with three biological replicates, each consisting of 10 seedlings.

RNA extraction and quantitative RT-PCR (RT-qPCR)

Total RNAs were prepared from seedlings using the Trizol RNA reagent (15596018, Thermo Fisher Scientific). First stand cDNAs were synthesized from 1 μg total RNA using the Maxima H Minus complementary DNA Synthesis Master Mix (M1682, Thermo Fisher Scientific). qPCRs were performed using the FastStart Essential DNA Green Master (06402712001, Roche) on a Real-Time PCR System (QuantStudio 6 Flex, Thermo Fisher Scientific). Primers for qPCRs are listed in Appendix Table S1. Quantifications of RT-qPCR data were based on three biological replicates using *GAPDH* as an internal control.

RNA-Seq and data analysis

Seedlings used in RNA-seq were grown under continuous light for 7 days and then treated with C-deprivation for 4 days. For each genotype, three biological replicates were included. Library preparation, sequencing, reads mapping, and differential expression analysis were performed at Novogene in Tianjin, China. Briefly, libraries were prepared using NEBNext® Ultra™ RNA Library Prep Kit for Illumina® (E7530L, New England Biolabs), and sequenced on an Illumina Novaseq platform. 150 bp paired-end reads were generated. Clean reads were aligned to the *Arabidopsis* reference genome (Araport11.Release.201606) using Hisat2 v2.0.5. Differential

expression analysis was performed using the DEseq2 R package. The resulting *P*-values were adjusted using Benjamini and Hochberg's approach. In each pair-wise comparison, genes with |log2 fold change| > 0.6 and an adjusted *P*-value (P_{adj}) < 0.01 found by DEseq2 were considered as differentially expressed. Enriched gene ontology (GO) terms were determined using functional annotation tools provided by DAVID Bioinformatics Resources 6.8 (https://david.ncifcrf.gov/tools.jsp).

Yeast two-hybrid assays

AD and BD vectors were co-transformed into the Y2H Gold yeast strain (630498, Takara Bio). Co-transformed yeast cells were selected on double dropout (DDO, SD-Leu/−Trp) medium. Liquid cultures grown from single colonies on DDO plates were adjusted to the same OD value. For each co-transformation, 5 µl liquid culture was spotted onto quadruple dropout (QDO, SD-Ade/-His/−Leu/−Trp) medium and QDO medium supplemented with 40 mg l^{-1} X-α-gal (630,462, Takara Bio) and incubated at 28°C. The growth of yeast colonies was monitored for 4–5 days. Empty *pGADT7* and *pGBKT7* plasmids served as negative controls.

Recombinant protein purification and GST pull-down assays

Expressions of recombinant proteins were induced in *Escherichia coli* strain BL21 (DE3) with 0.1 mM IPTG at 37°C (for GST, MBP-His, MBP-PIF5-His, and MBP-PIF4-His) or 30°C (for GST-ARF2) for 4 h. GST-ARF2 and GST were purified using the Glutathione Sepharose 4B resin (17-0756-01, GE Healthcare). MBP-PIF5-His, MBP-PIF4-His, and MBP-His were purified with the Ni Sepharose 6 Fast Flow resin (17-5318-02, GE Healthcare). Purified proteins were exchanged and concentrated with TBS buffer (25 mM Tris–HCl pH 7.2, 150 mM NaCl) using Pierce™ Protein Concentrator (88513 and 88502, Thermo Scientific). GST pull-down assays were performed with 5 µg GST or GST-ARF2 and 5 µg MBP-PIF5-His/MBP-PIF4-His using 10 µl Glutathione Sepharose 4B resin. Input and pull-down fractions were immunoblotted with anti-GST (ab19256, Abcam) and anti-His (ab18184, Abcam) antibodies. A protease inhibitor cocktail (04693132001, Roche) was added to 1× final concentration in all buffers used in recombinant protein purification and pull-down assays.

BiFC assays

Preparation and transient transfection of *Arabidopsis* leaf mesophyll protoplasts were performed as described (Yoo *et al*, 2007). In each assay, 200 µl protoplasts (2×10^5 ml^{-1}) were co-transfected with indicated *YN* and *YC* vectors (20 µg each) together with the nuclear marker vector *p35S:NLS-mCherry* (5 µg). Protoplasts were examined with a spinning-disk confocal system (Revolution WD, Andor) using a 100× 1.44 N.A. oil immersion objective (HCX PL Apo, Leica) 12 h after transfection. Confocal images were processed with the Fiji ImageJ software.

Co-Immunoprecipitation (Co-IP)

For Co-IP assays, 10 ml *phyB-101* mesophyll protoplasts (2×10^5 ml^{-1}) were co-transfected with 1 mg *p35S:ARF2-HA* together with 1 mg *p35S:PIF5-GFP*/*p35S:PIF4-GFP* or 0.1 mg *p35S:GFP*. After 12 h incubation in WI buffer (4 mM MES-KOH pH5.7, 0.5 M mannitol, and 20 mM KCl) in the dark, protoplasts were harvested (100 *g*, 2 min) and frozen in liquid nitrogen. Cell pellets were resuspended in 1 ml IP buffer (10 mM HEPES pH 8.0, 150 mM NaCl, 2.5 mM $MgCl_2$, 1% [v/v] Nonidet P-40, 0.5 mM EDTA, and 5% [v/v] glycerol), sonicated for 10 min (30 s on/off cycles) with Bioruptor Pico (Diagenode), incubated on ice for 30 min, and then centrifuged at 12,000 *g* for 5 min at 4°C. After centrifugation, the supernatant served as the input for Co-IP. IP was performed using magnetic GFP-Trap beads (gtma-20, ChromoTek). Input and IP fractions were immunoblotted with anti-GFP (632381, Takara Bio) and anti-HA (11867431001, Roche) antibodies. A protease inhibitor cocktail (04693132001, Roche) was added to 1× final concentration in all buffers used in sample preparation and Co-IP.

Chromatin immunoprecipitation (ChIP)-qPCR

ChIP assays were performed as described with minor modifications (Meng *et al*, 2018). Seven-day-old seedlings (Fig 7) or 7-day-old seedlings with an additional 3 days C-deprivation treatment (Fig 5) were used in ChIP assays. 3–4 g of seedlings were infiltrated with the crosslinking buffer (10 mM Tris–HCl pH 8.0, 0.4 M sucrose, 10 mM $MgCl_2$, 5 mM β-ME, 1 mM PMSF, and 1% formaldehyde) for 10 min under vacuum. Crosslinked seedlings were frozen and ground in liquid nitrogen. Nuclei purified by differential centrifugation in a discontinuous sucrose gradient were lysed in Nuclear Lysis Buffer (50 mM Tris–HCl pH 8.0, 10 mM EDTA, 1% [w/v] SDS, 1 mM PMSF, 1 × protease inhibitor cocktail). Chromatin was sheared with Bioruptor Pico (Diagenode). Chromatin complexes were immunoprecipitated with magnetic GFP-Trap beads (gtma-20, ChromoTek) at 4°C overnight with gentle agitation. After reverse crosslinking and proteinase K (EO0491, Thermo Fisher Scientific) digestion, immunoprecipitated DNAs were purified using the QIAquick PCR Purification Kit (28,104, Qiagen). Input and immunoprecipitated DNAs were adjusted to the same concentration prior to qPCR analysis. A *PP2A* fragment served as the non-binding control in ChIP-qPCRs. Fold enrichments were calculated with respect to the input. Primers used in ChIP-qPCRs are listed in Appendix Table S1.

Protoplast effector/reporter assays

In each assay, 200 µl WT mesophyll protoplasts (2×10^5 ml^{-1}) were co-transfected with WT or each mutant form of *pABS3:GFP* (20 µg) and *p35S:mCherry* (5 µg) with or without *p35S:ARF2-HA* (20 µg). Protoplasts were examined with a fluorescence microscope (DMi8, Leica) using a 20× objective lens (HC PL APO N.A. 0.80) 12 h after transfection. For each assay, relative GFP fluorescence signal intensity was measured in more than 100 transfected cells, i.e. cells expressing the *p35S:mCherry* transfection control, using Fiji-ImageJ software. All assays were repeated independently at least three times with similar results.

Accession numbers

Sequence data for the genes used in this study can be found in The *Arabidopsis* Information Resource (www.arabidopsis.org) under the

following accession numbers: *ABS3*, *AT4G29140*; *ABS4*, *AT1G58340*; *ABS3L1*, *AT5G19700*; *ABS3L2*, *AT5G52050*; *ARF2*, *AT5G62000*; *PIF5*, *AT3G59060*; *PIF4*, *AT2G43010*; *ORE1*, *AT5G39610*; *SGR1*, *AT4G22920*; *PIL1*, *AT2G46970*; *YUC8*, *AT4G28720*; *PP2A*, *AT1G13320*; *GAPDH*, *AT1G13440*.

Data availability

The RNA-seq raw data have been deposited to Sequence Read Archive (SRA; https://www.ncbi.nlm.nih.gov/sra) under the accession number PRJNA701129.

Expanded View for this article is available online.

Acknowledgements
This work was supported by grants from the National Natural Science Foundation of China (32070215 and 31870268 to FY, 32100291 to JM) and the Natural Science Basic Research Program of Shaanxi Province (2021JC-17 to XL). We thank the Teaching and Research Core Facility at the College of Life Sciences, Northwest A&F University, particularly Dr. Ningjuan Fan and Min Duan for technical assistance. We thank Dr. Kun-hsiang Liu for critical reading of the manuscript.

Author contributions
Hui Xue: Investigation; visualization. **Jingjing Meng:** Funding acquisition; investigation; visualization. **Pei Lei:** Investigation. **Yongxin Cao:** Investigation. **Xue An:** Investigation. **Min Jia:** Investigation. **Yan Li:** Investigation. **Haofeng Liu:** Investigation. **Jen Sheen:** Writing – review and editing. **Xiayan Liu:** Conceptualization; funding acquisition; writing – original draft. **Fei Yu:** Conceptualization; funding acquisition; writing – original draft; writing – review and editing.

In addition to the CRediT author contributions listed above, the contributions in detail are:

FY and XL conceived the study. FY, HX, and XL designed the experiments. HX, JM, PL, YC, XA, MJ, YL, and HL performed the experiments. HX and JM analyzed data and performed bioinformatics. FY and XL wrote the draft of the manuscript. JS reviewed and edited the manuscript. All authors discussed the results and commented on the manuscript.

Disclosure and competing interests statement
The authors declare that they have no conflict of interest.

References

Armstead I, Donnison I, Aubry S, Harper J, Hortensteiner S, James C, Mani J, Moffet M, Ougham H, Roberts L *et al* (2007) Cross-species identification of Mendel's I locus. *Science* 315: 73

Breeze E, Harrison E, McHattie S, Hughes L, Hickman R, Hill C, Kiddle S, Kim YS, Penfold CA, Jenkins D *et al* (2011) High-resolution temporal profiling of transcripts during *Arabidopsis* leaf senescence reveals a distinct chronology of processes and regulation. *Plant Cell* 23: 873 – 894

Buchanan-Wollaston V, Page T, Harrison E, Breeze E, Lim PO, Nam HG, Lin JF, Wu SH, Swidzinski J, Ishizaki K *et al* (2005) Comparative transcriptome analysis reveals significant differences in gene expression and signalling pathways between developmental and dark/starvation-induced senescence in *Arabidopsis*. *Plant J* 42: 567 – 585

Clough SJ, Bent AF (1998) Floral dip: a simplified method for agrobacterium-mediated transformation of *Arabidopsis thaliana*. *Plant J* 16: 735 – 743

Durian G, Sedaghatmehr M, Matallana-Ramirez LP, Schilling SM, Schaepe S, Guerra T, Herde M, Witte CP, Mueller-Roeber B, Schulze WX *et al* (2020) Calcium-dependent protein kinase CPK1 controls cell death by *in vivo* phosphorylation of senescence master regulator ORE1. *Plant Cell* 32: 1610 – 1625

Ellis CM, Nagpal P, Young JC, Hagen G, Guilfoyle TJ, Reed JW (2005) AUXIN RESPONSE FACTOR1 and AUXIN RESPONSE FACTOR2 regulate senescence and floral organ abscission in *Arabidopsis thaliana*. *Development* 132: 4563 – 4574

Guo Y, Gan SS (2012) Convergence and divergence in gene expression profiles induced by leaf senescence and 27 senescence-promoting hormonal, pathological and environmental stress treatments. *Plant Cell Environ* 35: 644 – 655

Guo Y, Gan SS (2014) Translational researches on leaf senescence for enhancing plant productivity and quality. *J Exp Bot* 65: 3901 – 3913

Guo Y, Cai Z, Gan S (2004) Transcriptome of *Arabidopsis* leaf senescence. *Plant, Cell & Environment* 27: 521 – 549

Hornitschek P, Kohnen MV, Lorrain S, Rougemont J, Ljung K, Lopez-Vidriero I, Franco-Zorrilla JM, Solano R, Trevisan M, Pradervand S *et al* (2012) Phytochrome interacting factors 4 and 5 control seedling growth in changing light conditions by directly controlling auxin signaling. *Plant J* 71: 699 – 711

Jia M, Liu X, Xue H, Wu Y, Shi L, Wang R, Chen Y, Xu N, Zhao J, Shao J *et al* (2019) Noncanonical ATG8-ABS3 interaction controls senescence in plants. *Nat Plants* 5: 212 – 224

Jin JP, Tian F, Yang DC, Meng YQ, Kong L, Luo JC, Gao G (2017) PlantTFDB 4.0: Toward a central hub for transcription factors and regulatory interactions in plants. *Nucleic Acids Res* 45: D1040 – D1045

Kamranfar I, Xue GP, Tohge T, Sedaghatmehr M, Fernie AR, Balazadeh S, Mueller-Roeber B (2018) Transcription factor RD26 is a key regulator of metabolic reprogramming during dark-induced senescence. *New Phytol* 218: 1543 – 1557

Keller MM, Jaillais Y, Pedmale UV, Moreno JE, Chory J, Ballare CL (2011) Cryptochrome 1 and phytochrome B control shade-avoidance responses in *Arabidopsis* via partially independent hormonal cascades. *Plant J* 67: 195 – 207

Kim JH, Woo HR, Kim J, Lim PO, Lee IC, Choi SH, Hwang D, Nam HG (2009) Trifurcate feed-forward regulation of age-dependent cell death involving miR164 in *Arabidopsis*. *Science* 323: 1053 – 1057

Kim J, Woo HR, Nam HG (2016) Toward systems understanding of leaf senescence: an integrated multi-omics perspective on leaf senescence research. *Mol Plant* 9: 813 – 825

Kim H, Kim HJ, Vu QT, Jung S, McClung CR, Hong S, Nam HG (2018) Circadian control of ORE1 by PRR9 positively regulates leaf senescence in *Arabidopsis*. *Proc Natl Acad Sci USA* 115: 8448 – 8453

Leivar P, Monte E (2014) PIFs: systems integrators in plant development. *Plant Cell* 26: 56 – 78

Leivar P, Monte E, Al-Sady B, Carle C, Storer A, Alonso JM, Ecker JR, Quail PH (2008a) The *Arabidopsis* phytochrome-interacting factor PIF7, together with PIF3 and PIF4, regulates responses to prolonged red light by modulating phyB levels. *Plant Cell* 20: 337 – 352

Leivar P, Monte E, Oka Y, Liu T, Carle C, Castillon A, Huq E, Quail PH (2008b) Multiple phytochrome-interacting bHLH transcription factors repress premature seedling photomorphogenesis in darkness. *Curr Biol* 18: 1815 – 1823

Li H, Johnson P, Stepanova A, Alonso JM, Ecker JR (2004) Convergence of signaling pathways in the control of differential cell growth in *Arabidopsis*. *Dev Cell* 7: 193 – 204

Li L, Ljung K, Breton G, Schmitz RJ, Pruneda-Paz J, Cowing-Zitron C, Cole BJ, Ivans LJ, Pedmale UV, Jung HS *et al* (2012) Linking photoreceptor excitation to changes in plant architecture. *Genes Dev* 26: 785 – 790

Li Y, Deng M, Liu H, Li Y, Chen Y, Jia M, Xue H, Shao J, Zhao J, Qi Y *et al* (2021) ABNORMAL SHOOT 6 interacts with KATANIN 1 and SHADE AVOIDANCE 4 to promote cortical microtubule severing and ordering in *Arabidopsis*. *J Integr Plant Biol* 63: 646 – 661

Lichtenthaler KH (1987) [34] chlorophylls and carotenoids: pigments of photosynthetic biomembranes. In *Plant Cell Membranes*, L Packer, R Douce (eds), pp 350 – 382. Amsterdam: Elsevier

Liebsch D, Keech O (2016) Dark-induced leaf senescence: new insights into a complex light-dependent regulatory pathway. *New Phytol* 212: 563 – 570

Lim PO, Lee IC, Kim J, Kim HJ, Ryu JS, Woo HR, Nam HG (2010) Auxin response factor 2 (ARF2) plays a major role in regulating auxin-mediated leaf longevity. *J Exp Bot* 61: 1419 – 1430

Lin JF, Wu SH (2004) Molecular events in senescing *Arabidopsis* leaves. *Plant J* 39: 612 – 628

Lorrain S, Allen T, Duek PD, Whitelam GC, Fankhauser C (2008) Phytochrome-mediated inhibition of shade avoidance involves degradation of growth-promoting bHLH transcription factors. *Plant J* 53: 312 – 323

Meng J, Wang L, Wang J, Zhao X, Cheng J, Yu W, Jin D, Li Q, Gong Z (2018) METHIONINE ADENOSYLTRANSFERASE4 mediates DNA and histone methylation. *Plant Physiol* 177: 652 – 670

Moreno-Mateos MA, Vejnar CE, Beaudoin JD, Fernandez JP, Mis EK, Khokha MK, Giraldez AJ (2015) CRISPRscan: designing highly efficient sgRNAs for CRISPR-Cas9 targeting *in vivo*. *Nat Methods* 12: 982 – 988

Oh E, Zhu JY, Bai MY, Arenhart RA, Sun Y, Wang ZY (2014) Cell elongation is regulated through a central circuit of interacting transcription factors in the *Arabidopsis* hypocotyl. *Elife* 3: e03031

Okushima Y, Mitina I, Quach HL, Theologis A (2005) AUXIN RESPONSE FACTOR 2 (ARF2): a pleiotropic developmental regulator. *Plant J* 43: 29 – 46

O'Malley RC, Huang SSC, Song L, Lewsey MG, Bartlett A, Nery JR, Galli M, Gallavotti A, Ecker JR (2016) Cistrome and Epicistrome features shape the regulatory DNA landscape. *Cell* 165: 1280 – 1292

Paik I, Kathare PK, Kim JI, Huq E (2017) Expanding roles of PIFs in signal integration from multiple processes. *Mol Plant* 10: 1035 – 1046

Park BS, Yao T, Seo JS, Wong ECC, Mitsuda N, Huang CH, Chua NH (2018) *Arabidopsis* NITROGEN LIMITATION ADAPTATION regulates ORE1 homeostasis during senescence induced by nitrogen deficiency. *Nat Plants* 4: 898 – 903

Pedmale UV, Huang SC, Zander M, Cole BJ, Hetzel J, Ljung K, Reis PAB, Sridevi P, Nito K, Nery JR *et al* (2016) Cryptochromes interact directly with PIFs to control plant growth in limiting blue light. *Cell* 164: 233 – 245

Pfeiffer A, Shi H, Tepperman JM, Zhang Y, Quail PH (2014) Combinatorial complexity in a transcriptionally centered signaling hub in *Arabidopsis*. *Mol Plant* 7: 1598 – 1618

Pham VN, Kathare PK, Huq E (2018) Phytochromes and phytochrome interacting factors. *Plant Physiol* 176: 1025 – 1038

Richter R, Behringer C, Zourelidou M, Schwechheimer C (2013) Convergence of auxin and gibberellin signaling on the regulation of the GATA transcription factors GNC and GNL in *Arabidopsis thaliana*. *Proc Natl Acad Sci USA* 110: 13192 – 13197

Sakuraba Y, Jeong J, Kang MY, Kim J, Paek NC, Choi G (2014) Phytochrome-interacting transcription factors PIF4 and PIF5 induce leaf senescence in *Arabidopsis*. *Nat Commun* 5: 4636

Schippers JH, Schmidt R, Wagstaff C, Jing HC (2015) Living to die and dying to live: the survival strategy behind leaf senescence. *Plant Physiol* 169: 914 – 930

Schruff MC, Spielman M, Tiwari S, Adams S, Fenby N, Scott RJ (2006) The AUXIN RESPONSE FACTOR 2 gene of *Arabidopsis* links auxin signalling, cell division, and the size of seeds and other organs. *Development* 133: 251 – 261

Shen Y, Khanna R, Carle CM, Quail PH (2007) Phytochrome induces rapid PIF5 phosphorylation and degradation in response to red-light activation. *Plant Physiol* 145: 1043 – 1051

Shor E, Paik I, Kangisser S, Green R, Huq E (2017) PHYTOCHROME INTERACTING FACTORS mediate metabolic control of the circadian system in *Arabidopsis*. *New Phytol* 215: 217 – 228

Song Y, Yang C, Gao S, Zhang W, Li L, Kuai B (2014) Age-triggered and dark-induced leaf senescence require the bHLH transcription factors PIF3, 4, and 5. *Mol Plant* 7: 1776 – 1787

Song Q, Ando A, Xu D, Fang L, Zhang T, Huq E, Qiao H, Deng XW, Chen ZJ (2018) Diurnal down-regulation of ethylene biosynthesis mediates biomass heterosis. *Proc Natl Acad Sci USA* 115: 5606 – 5611

Tiwari SB, Hagen G, Guilfoyle T (2003) The roles of auxin response factor domains in auxin-responsive transcription. *Plant Cell* 15: 533 – 543

Ulmasov T, Hagen G, Guilfoyle TJ (1999) Activation and repression of transcription by auxin-response factors. *Proc Natl Acad Sci USA* 96: 5844 – 5849

Wang L, Hua D, He J, Duan Y, Chen Z, Hong X, Gong Z (2011) Auxin response Factor2 (ARF2) and its regulated homeodomain gene HB33 mediate abscisic acid response in *Arabidopsis*. *PLoS Genet* 7: e1002172

Wang R, Liu X, Liang S, Ge Q, Li Y, Shao J, Qi Y, An L, Yu F (2015a) A subgroup of MATE transporter genes regulates hypocotyl cell elongation in *Arabidopsis*. *J Exp Bot* 66: 6327 – 6343

Wang ZP, Xing HL, Dong L, Zhang HY, Han CY, Wang XC, Chen QJ (2015b) Egg cell-specific promoter-controlled CRISPR/Cas9 efficiently generates homozygous mutants for multiple target genes in *Arabidopsis* in a single generation. *Genome Biol* 16: 144

Woo HR, Koo HJ, Kim J, Jeong H, Yang JO, Lee IH, Jun JH, Choi SH, Park SJ, Kang B *et al* (2016) Programming of plant leaf senescence with temporal and inter-organellar coordination of transcriptome in *Arabidopsis*. *Plant Physiol* 171: 452 – 467

Woo HR, Kim HJ, Lim PO, Nam HG (2019) Leaf senescence: systems and dynamics aspects. *Annu Rev Plant Biol* 70: 347 – 376

Yang J, Worley E, Udvardi M (2014) A NAP-AAO3 regulatory module promotes chlorophyll degradation via ABA biosynthesis in Arabidopsis leaves. *The Plant Cell*, 26: 4862 – 4874

Yoo SD, Cho YH, Sheen J (2007) *Arabidopsis* mesophyll protoplasts: a versatile cell system for transient gene expression analysis. *Nat Protoc* 2: 1565 – 1572

Zentgraf U (2019) Tug-of-war during senescence. *Nat Plants* 5: 129 – 130

Zhang Y, Liu Z, Chen Y, He JX, Bi Y (2015) PHYTOCHROME-INTERACTING FACTOR 5 (PIF5) positively regulates dark-induced senescence and chlorophyll degradation in *Arabidopsis*. *Plant Sci* 237: 57 – 68

Zhao S, Zhang ML, Ma TL, Wang Y (2016) Phosphorylation of ARF2 relieves its repression of transcription of the K^+ transporter gene HAK5 in response to low potassium stress. *Plant Cell* 28: 3005 – 3019

Zhuo M, Sakuraba Y, Yanagisawa S (2020) A Jasmonate-activated MYC2-Dof2.1-MYC2 transcriptional loop promotes leaf senescence in *Arabidopsis*. *Plant Cell* 32: 242 – 262